NJC

RSC Publishing

PAPER

View Article Online
View Journal

Published on 11 October 2013. Downloaded by Laurentian University on 04/11/2013 00:26:56.

Cite this: DOI: 10.1039/c3nj00750b

Ratiometric fluorescent Zn^{2+} and In^{3+} receptors of fused pyrazine with an aminopropanol chain in acetonitrile†

Katarzyna Ostrowska,*[a] Alicja Kaźmierska,[a] Maria Rąpała-Kozik[b] and Justyna Kalinowska-Tłuścik‡[a]

Received (in Montpellier, France)
7th July 2013,
Accepted 10th October 2013

DOI: 10.1039/c3nj00750b

www.rsc.org/njc

A series of new potential intramolecular charge transfer ICT fluorescent receptors of Zn^{2+}, Cd^{2+}, Hg^{2+}, Ga^{3+}, In^{3+}, and Tl^{3+} ions based on *N*-aryl or *N*-alkyl variously fused pyridopyrrolopyrazine or pyrrolo-[2,3-*b*]quinoxaline with an integrated donor group, such as 3-aminopropanol, were synthesized and verified. Among [*N*, *N*, *O*] tridentate donors **4a**, **6a–d**, **10a**, **12e**, and **14e**, only the integrated fluorophore-receptors with the nitrogen atom at the N-5 position of heterocyclic systems, pyrido[2,3-*b*]-pyrrolo[2,3-*e*]pyrazine **6a**, selectively respond to zinc and indium with significant fluorescent enhancement and different mechanisms of binding. The first example of *Z* to *E* interconversion of enaminone forms of a ligand responsible for Zn^{2+} complex fluorescence enhancement was documented.

Introduction

One of the most challenging fields in organic and supramolecular chemistry is development of the fluorescent molecular sensors, especially for heavy and transition metal ions.[1–11] Current fluorescent molecular sensors for metal ions usually contain a fluorophore and a receptor, which can form an integrated or a spaced fluorophore–receptor system. Receptors include *N*-, *O*-, or *S*-donor groups, which are responsible for selective metal ion binding. The fluorophores with conjugated π-electron systems change their photophysical properties upon complexation, signalling binding with metal ions. The emitted signals are detected as the enhancement of fluorescent emission with a red or blue shift of the emitted band or the quenching of the fluorescence. Azaheteroarenes, containing one or more heterocyclic nitrogen atoms, such as pyridine,[12,13] quinoline,[14–20] quinoxaline,[21,22] acridine,[23–27] indole,[28–30] and carbazole[31,32] are usually used as fluorogenic sensor components. These heterocyclic systems with separated or integrated receptor units containing amino, imino, amido, hydroxy, alkoxy, carbonyl, or carboxyl groups and a metal ion form five- or six-membered chelate rings with binding mode 1 : 1, 2 : 1, or even 3 : 1.[33] The connection between the ionophore and the fluorophore is essential for signalling and recognition function. The cation-induced photophysical changes are mainly based on photoinduced electrons, protons or charge transfer and excimer formation. The general classification of fluorescent sensors is connected with the origin of photoinduced changes such as photoinduced electron transfer cation sensors (PET) or photoinduced charge transfer cation sensors (ICT). Usually the cation sensors (ICT) contain conjugated electron-donating and electron-withdrawing groups forming an intramolecular push–pull electronic system. During the formation of the complex the metal cation interacts with the donor or acceptor moiety, which affects the efficiency of intramolecular charge transfer upon excitation by light.

8-arylsulphonamide (Zinquin)[13] or 8-carboxamide derivatives of quinoline (AQZ)[15] are the most widely used ICT fluorescent sensors for zinc cations in biological samples (Fig. 1). Sensors contain electron-acceptor amido groups and electron-donors with the N-1 quinoline nitrogen atom. When the metal ion is bound to an electron-withdrawing amido group, the complexation is associated with the deprotonation of the amine leading to an enhanced ICT process from the donor to the acceptor upon excitation by light. The replacement of hydrogen by the zinc ion and the formation of a five-membered chelate

[a] Faculty of Chemistry, Jagiellonian University, R. Ingardena 3, PL-30060 Kraków, Poland. E-mail: ostrowsk@chemia.uj.edu.pl; Fax: +48-12-63-40-515
[b] Faculty of Biochemistry, Biophysics and Biotechnology, Jagiellonian University, Gronostajowa 7, PL-30387 Kraków, Poland

† Electronic supplementary information (ESI) available: 2D fluorescence spectra of **4a**, **4a-Hg**, **6a**, **6a-Zn**, **6a-In**, **6a-Hg**, **12e**, and **14e**. Fluorescence spectra of **4a**, **6**, **10a**, **12e**, and **14e** (10 μM) in CH_3CN with 1 equiv. of Cd^{2+}. Fluorescence spectra of **4a**, **6**, **10a**, **12e**, and **14e** (10 μM) in CH_3CN with 1 equiv. of Hg^{2+}. Fluorescence titration of **6a** with $Zn(acac)_2$, $Zn(OAc)_2$, and $ZnCl_2$. ^1H and ^{13}C NMR spectra of compounds **6a–d**, **8a**, **9a**, **10a**, **12e,f**, and **14e,f**. Partial ^1H NMR titration spectra of **6a** with $Zn(acac)_2$ in CD_3CN and DMSO-d_6. Conformational and intermolecular interaction analysis of crystal structures of **6a** and **12e**. CCDC 890198 and 890197. For ESI and crystallographic data in CIF or other electronic format see DOI: 10.1039/c3nj00750b

‡ For crystal structure information, e-mail: kalinows@chemia.uj.edu.pl.

Published on 11 October 2013. Downloaded by Laurentian University on 04/11/2013 00:26:56.

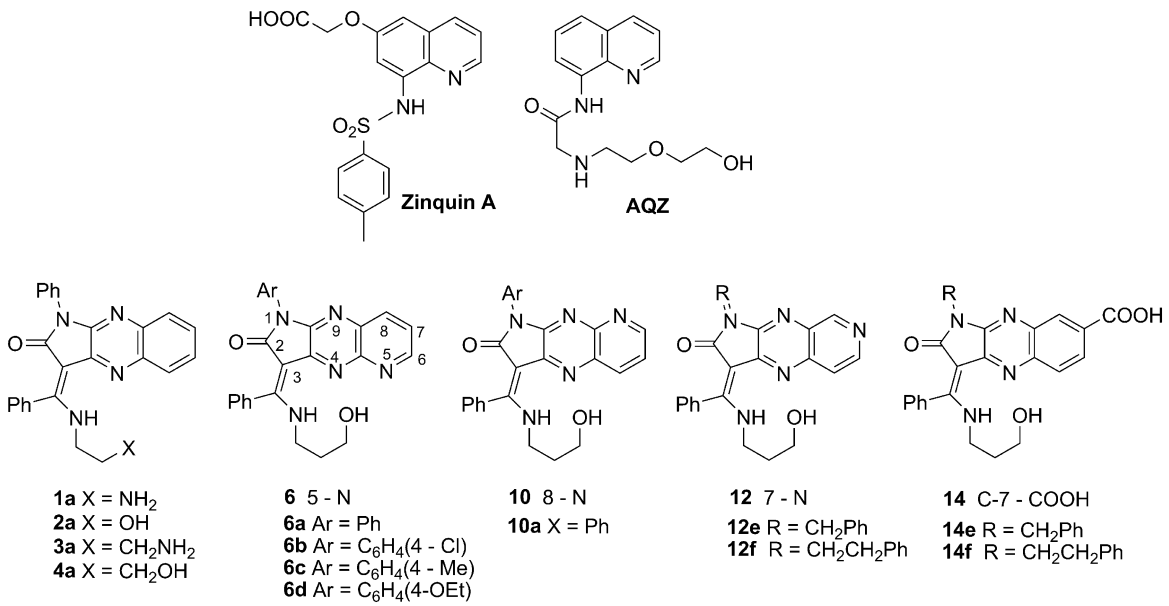

Fig. 1 General structures of the studied chemosensors.

ring broaden the conjugation of the π-system resulting in Stokes red-shift of the absorption spectra. In addition to this shift a 300-fold increase in their fluorescence intensity upon chelation of zinc is observed.[34]

We previously designed ICT integrated fluorophore–receptor sensors **1a–4a** for zinc ions, with (*E*/*Z*)-3-[(alkylamino)phenylmethylidene]-pyrrolo[2,3-*b*]quinoxaline as the fluorogenic component and amino, hydroxyl, aminoalkyl or hydroxyalkyl groups as additional receptors (Fig. 1).[35] Among these [*N*, *N*, *N*] or [*N*, *N*, *O*] tridentate ligands **1a–4a**, compound **3a** showed the ratiometric turn-on fluorescence response toward zinc cations within the working zinc concentration range of K_d = 3.77 ± 0.51 μM and a binding stoichiometry of 1 : 1. This push–pull (*E*/*Z*)-enamine undergoes deprotonation while binding zinc cations, yielding a red-shifted excitation wavelength with induced charge transfer signal transduction (ICT).[35]

The electronegativity of the oxygen atom in the carbonyl group of imide causes the delocalization of N-1 or enamine nitrogen's lone pairs into the π system, leading to formation of zwitterions **A** or **B**, respectively (Scheme 1). Form **B** is stabilised by an internal hydrogen bond. The positive charge on iminium ions in form **A** may be modulated by electron-donating or electron-withdrawing character of these groups attached to N-1. The electron-donating group could decrease and stabilize positive charge on iminium ions, or the electron-withdrawing group could increase the positive charge and enhance the dipole moment of **4a**. Deprotonation and coordination of the zinc atom, more electropositive than hydrogen, to the nitrogen of the conjugated enaminone moiety and the N-4 nitrogen donor of quinoxaline changes the distribution of electronic charge in the push–pull system. Formation of the six-membered chelate ring extends π-conjugation resulting in a cation-induced red shift of the absorption spectrum and fluorescence emission upon excitation by light.

In this paper, we report the syntheses and photophysical properties of various new fluorophores: aryl or alkylphenyl substituted at the N-1 position of pyridopyrrolopyrazine (**6**),[36] (**10**), (**12**),[37] and pyrrolo[2,3-*b*]quinoxaline-7-carboxylic acid (**14**),[37] integrated with 3-aminopropan-1-ol upon complexation with biologically[12–20,25,26,28,31,38–40] and environmentally[20,24,27,32,38,39] important metal ions, such as Zn^{2+}, Cd^{2+}, Hg^{2+}, Ga^{3+}, In^{3+}, and Tl^{3+}.

Results and discussion

Ligands **6**, **10**, **12**, and **14** were efficiently synthesised according to our previously published procedure, using ketones **5**, **9a**, **11f**, **11e** and salt of the latter or a regioisomeric mixture of keto

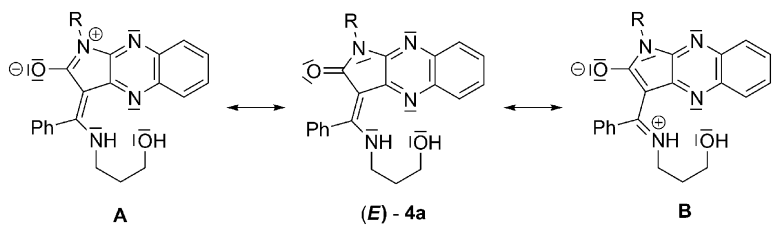

Scheme 1 Zwitterionic resonance structures of receptor **4a**.

This journal is © The Royal Society of Chemistry and the Centre National de la Recherche Scientifique 2013

Published on 11 October 2013. Downloaded by Laurentian University on 04/11/2013 00:26:56.

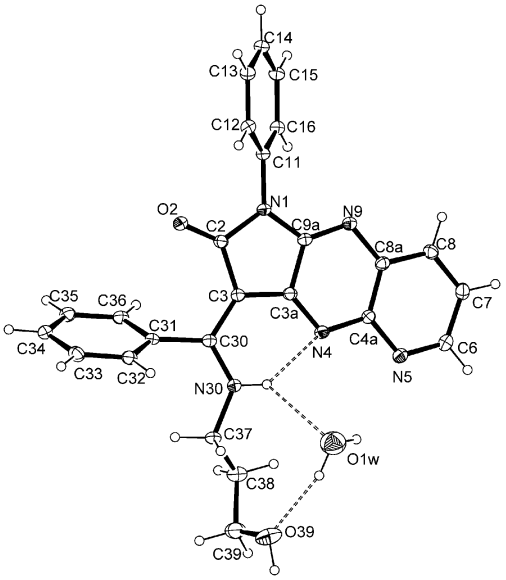

Fig. 2 Crystal structure of **6a** as a monohydrate, showing the atom labelling scheme. Displacement ellipsoids of non-hydrogen atoms are drawn at the 30% probability level. H atoms are presented as small spheres with an arbitrary radius. Dashed lines represent a hydrogen bond system observed within the asymmetric unit.

acids **13** with 3-aminoalkohol as reagents (Scheme 2).[35] Regioisomer **9a** was obtained using a multistep method exploiting the *exo-enol* tautomerism of **7a** in CH_2Cl_2 to furnish 3-amino-*N*-(2-amino-3-pyridyl)-pyrrolidinedione **8a**, which was then cyclized in EtOH. Aminoalcohol was used in excess, acting as both reagent and solvent and reacting regioselectively at the benzoyl carbon atom. The reaction was carried out at room temperature for 5 days while the product precipitated. To shorten the reaction time for **6a**, we modified this procedure by adding propanol to the reaction mixture and heating the starting materials at 50 °C for 3 h. Compounds **6c** and **14f** crystallise with one molecule of aminopropanol.

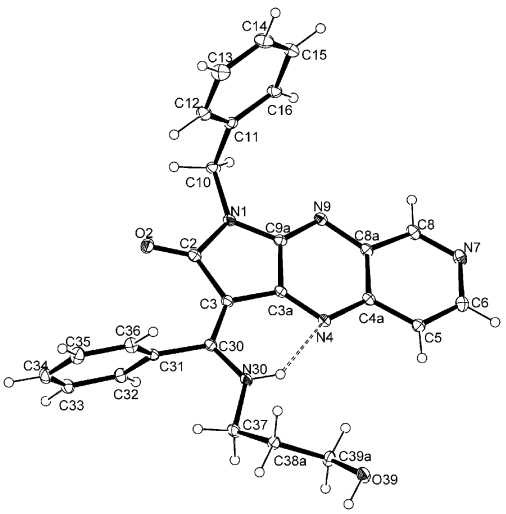

Fig. 3 Crystal structure of **12e**, specifically, the more abundant conformation with an occupancy of 88.4%, showing the atom labelling scheme. Displacement ellipsoids of non-hydrogen atoms are drawn at the 30% probability level. H atoms are presented as small spheres of an arbitrary radius. The dashed line represents an intramolecular hydrogen bond.

According to our previous results, we obtained mixtures of the *E*/*Z* diastereoisomers of **6a–6d**, **10a**, **12e**, **12f** and **14e**, **14f**, with *E*-isomers predominating in solution (Table 1). The presence of a nitrogen atom at N-5 for **6** effectively shifts the *E*/*Z* equilibrium in $CDCl_3$ to *E*-form, plausibly due to formation of an additional intramolecular hydrogen bond between the N-5 nitrogen atom and the hydroxyl group in solution. In the case of the mixture of regioisomeric 6- and 7-carboxylic acids of 3-benzoylpyrrolo[2,3-*b*]quinoxaline **13**, only the regioisomeric 7-substituted products **14e** and **14f** were isolated.

X-ray structure analysis[41–48] of (*E*)-**6a** and (*E*)-**12e** showed the stabilisation of the configuration in the solid. For both structures, an intramolecular hydrogen bond N30–H30···N4 is observed H30···N4 = 2.16(3) Å, N30···N4 = 2.837(3) Å and N30–H30···N7 = 137(3)° for **6a** (Fig. 2) and H30···N4 = 2.162(17) Å, N30···N4 = 2.894(1) Å and N30–H30···N7 = 138.0(14)° for **12e** (Fig. 3).

The absorption and emission data for the studied compounds are listed in Table 2. The quantum yields (Φ_n) for compounds **5a,d**, **6a,d** and **9a**, **10a**, **12e,f**, and **14e,f** were determined in chloroform and acetonitrile using 1 mM stock solution prepared in DMSO. The lifetimes (τ_n) for all of the analysed compounds were obtained in chloroform. The solubility of the compounds was the basis of the solvent selection. In principle, no significant differences were observed in the absorption and emission spectra in the two solvents for compounds **6a**, **9a**, **10a**, **12e**, and **14e**. The UV/Vis spectra of all enamines **6**, **10a**, **12e,f**, and **14e,f** exhibited two maxima (376–388 and 393–402 nm) with equal molar absorption coefficients.

All enamines exhibit weak fluorescence properties regardless of the various azaheteroarene fluorophores. To verify the sensing abilities of integrated fluorophore–receptor sensors for divalent and trivalent Zn^{2+}, Cd^{2+}, Hg^{2+}, Ga^{3+}, In^{3+}, Tl^{3+} ions, we performed a detailed spectrophotometric study. The most effective turn-on fluorescence response among *N*-aryl or *N*-alkyl variously fused pyridopyrrolopyrazine or pyrrolo[2,3-*b*]quinoxaline for Zn^{2+} and In^{3+} is exhibited by **6a** (Fig. 4a and b). Trivalent indium and divalent zinc ions have comparable Pauling's ionic radius and electronegativity. Additionally these ions have confined d^{10} electron shells. Thus, the trivalent indium cation should form a more stable complex with **6a** in comparison with divalent zinc ions.[49] Different emission profiles for **6a-Zn^{2+}** and **6a-In^{3+}** suggest, however, different mechanisms of complexation responsible for fluorescence enhancement.

We detected very low fluorescence response of all azaheteroarenes to Cd^{2+}, and Hg^{2+} ions (ESI†) and lack of any changes for Ga^{3+}, Tl^{1+}, and Tl^{3+} ions.

The [*N*, *N*, *O*] tridentate ligands **6a**, **6b** are fluorescent for zinc ions, most likely due to the electronic effect of the most electron-withdrawing phenyl and 4-chlorophenyl groups at the N-1 position and the additional integrated nitrogen donor at the N-5 position of the fused heterocyclic system. The presence of the less electron-withdrawing methyl and ethoxyl group at

Published on 11 October 2013. Downloaded by Laurentian University on 04/11/2013 00:26:56.

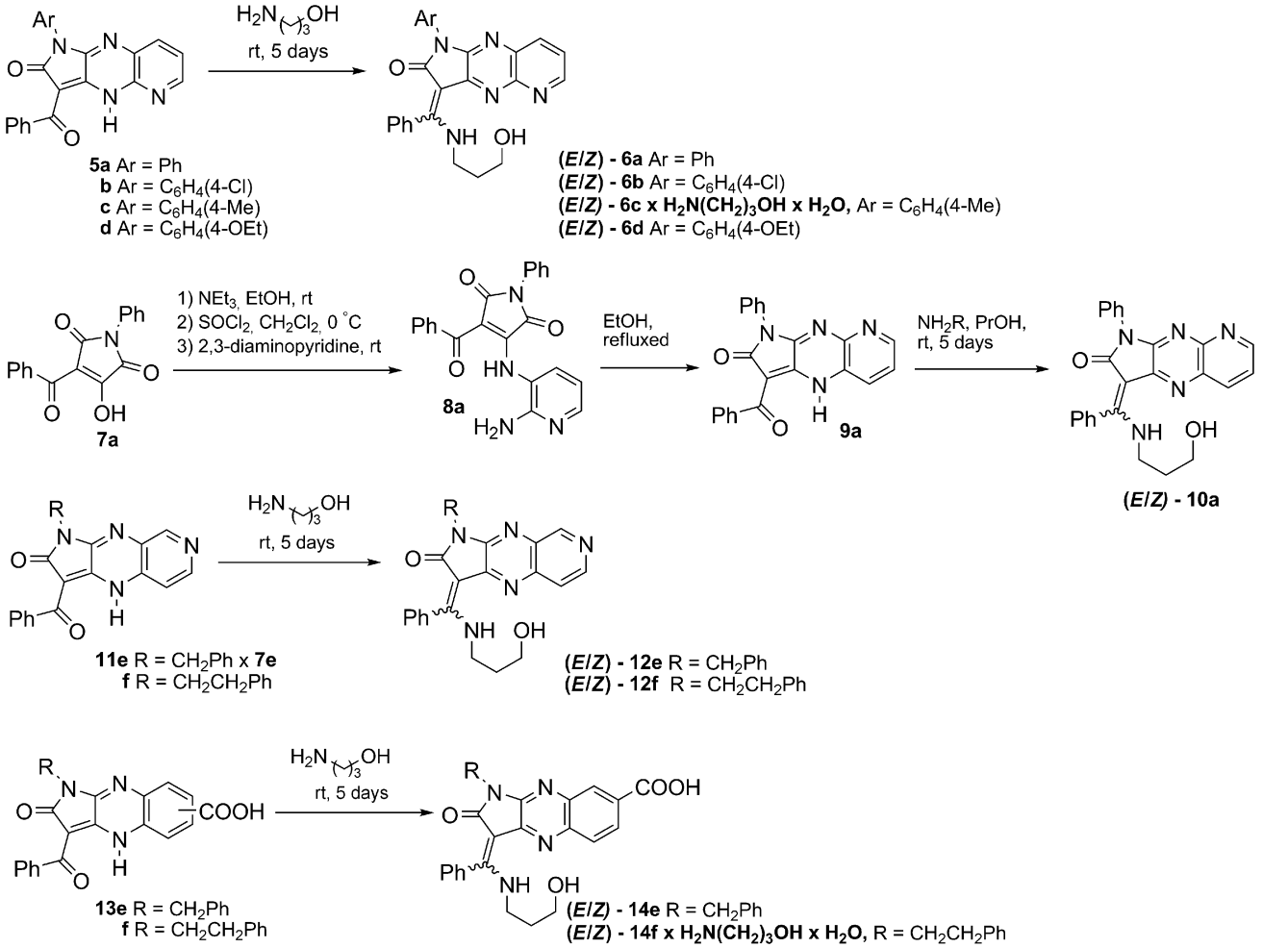

Scheme 2 *N*-Alkyl enamination of 3-benzoylpyridopyrrolopyrazine **5a–d**, **9a**, **11e,f** and pyrrolo[2,3-*b*]quinoxaline-7-carboxylic acid derivatives **13e,f**.

the 4-substituted phenyl substituent for **6c** and **6d** amplifies the electron-donating character of the amide nitrogen atom. That reduces the dipole moment of the fluorophore and degree of charge transfer upon excitation of light which is in accordance with the literature.[50]

In contrast to the photooptical properties of reported *N*-methylnaphthalimide[51,52] or *N*-methylindole[53] derivatives, the electron-donor group at the N-1 position, such as benzyl for **12e** and **14e** reduces the degree of charge transfer responsible for fluorescence enhancement. The possible explanation for that difference in photooptical properties of fused *N*-alkyl imides may be connected not only with the electron-donating character of alkyl substituents but also with the restriction of π-conjugation. It seems probable that extended π-conjugation of the pyridopyrrolopyrazine with the aryl group at the N-1 position is essential for switching upon binding the zinc ion. However, confirmation of this photooptical phenomenon requires additional study. Other pyridopyrrolopyrazine derivatives **10a** and pyrrolo[2,3-*b*]quinoxaline **4a** as [*N*, *N*, *O*] tridentate ligands do not exhibit a turn-on fluorescence response. The quite similar behaviour of these tridentate ligands is not surprising because the receptor component, 3-aminopropanol and lack of additional donor nitrogen at N-5, are the same.

Table 1 The results of *N*-alkyl enamination leading to an (*E*/*Z*) equilibrium of **6**, **10a**, **12e,f**, and **14e,f** in $CDCl_3$, DMSO-d_6, and CD_3CN

	Yield [%]	*E*/*Z* ratio $CDCl_3$	*E*/*Z* ratio DMSO-d_6	*E*/*Z* ratio CD_3CN
6a Ar = Ph	98	10 : 1	2.7 : 1	2.6 : 1
6b Ar = C_6H_4(4-Cl)	98	8.7 : 1	3.2 : 1	
6c Ar = C_6H_4(4-Me)	82	8.7 : 1	3 : 1	
6d Ar = C_6H_4(4-OEt)	51	7.1 : 1	2.9 : 1	
10a Ar = Ph, R = $(CH_2)_3OH$	75	2 : 1	1.9 : 1	
12e Ar = Bn	35	2 : 1	2.1 : 1	
12f Ar = CH_2CH_2Ph	21	2.6 : 1	2.2 : 1	
14e[a] Ar = Bn	42		2.2 : 1	
14f[a] Ar = CH_2CH_2Ph	31		2.8 : 1	

[a] Compound is barely soluble in $CDCl_3$.

To study the influence of anions on the fluorescent spectra of **6a-Zn**, we performed experiments between **6a** (10 μM, Fig. 5) and different salts such as $ZnSO_4$, $ZnCl_2$, $Zn(NO_3)_2$, $Zn(OTf)_2$, $Zn(OAc)_2$, and $Zn(acac)_2$ (10 μM). The experiment showed that the fluorescent enhancement of **6a-Zn** increases in accordance with the basicity of anions. When anions are bound to metals in complexes their basicity may modulate the fluorescence intensity *via* changing the electron density on the donor group

 This journal is © The Royal Society of Chemistry and the Centre National de la Recherche Scientifique 2013

Published on 11 October 2013. Downloaded by Laurentian University on 04/11/2013 00:26:56.

Table 2 Photophysical properties of the analysed compounds

	λ_{abs} [nm]	ε [10^3 M^{-1} cm^{-1}]	λ_{em} [a] [nm]	Φ_n [b,c]	τ_n [c,d] [s]
5a	396[d]	24.16 ± 1.71	456	0.023 ± 0.0006	$5.38 \times 10^{-10} \pm 1.01 \times 10^{-11}$
5b	400[d]	26.84 ± 1.54	456	0.007 ± 0.0010	$5.08 \times 10^{-10} \pm 7.58 \times 10^{-12}$
5c	396[d]	29.62 ± 2.31	n.f.	—	n.f.
5d	396[d]	30.18 ± 2.53	n.f.	—	n.f.
6a	388, 408[d]	28.25 ± 2.31	444	0.0077 ± 0.0005	$5.36 \times 10^{-10} \pm 7.92 \times 10^{-11}$
6b	388, 408[d]	22.69 ± 2.88	444	0.0083 ± 0.0004	$2.17 \times 10^{-10} \pm 1.01 \times 10^{-11}$
6c	388, 408[d]	14.35 ± 2.69	444	0.0073 ± 0.0005	$2.57 \times 10^{-10} \pm 4.05 \times 10^{-12}$
6d	388, 408[d]	27.87 ± 1.77	444	0.0027 ± 0.0008	$2.21 \times 10^{-10} \pm 7.60 \times 10^{-12}$
9a	396[e]	27.61 ± 1.72	457	0.0560 ± 0.0008	$8.34 \times 10^{-10} \pm 1.24 \times 10^{-11}$
10a	382, 398[e]	31.17 ± 1.99	440	0.0021 ± 0.0005	$3.27 \times 10^{-10} \pm 5.75 \times 10^{-11}$
12e	376, 393[e]	30.80 ± 5.07	438	0.0018 ± 0.0006	$1.03 \times 10^{-10} \pm 2.51 \times 10^{-12}$
12f	376, 393[e]	28.54 ± 3.30	438	0.0015 ± 0.0004	$1.01 \times 10^{-10} \pm 2.89 \times 10^{-11}$
14e	376, 392[e]	28.25 ± 1.38	438	0.0010 ± 0.0005	$3.92 \times 10^{-10} \pm 7.09 \times 10^{-12}$
14f	386, 402[e]	31.40 ± 1.83	440	0.0021 ± 0.0004	$1.74 \times 10^{-10} \pm 9.12 \times 10^{-11}$

[a] n.f.: non-detectable fluorescent emission. [b] The fluorescence quantum yields (Φ_n) were estimated from the corrected fluorescence spectra using 9,10-diphenylanthracene in cyclohexane (Φ_s = 0.90) as the standard. [c] Average of three measurements. [d] Measurements in $CHCl_3$. [e] Measurements in CH_3CN.

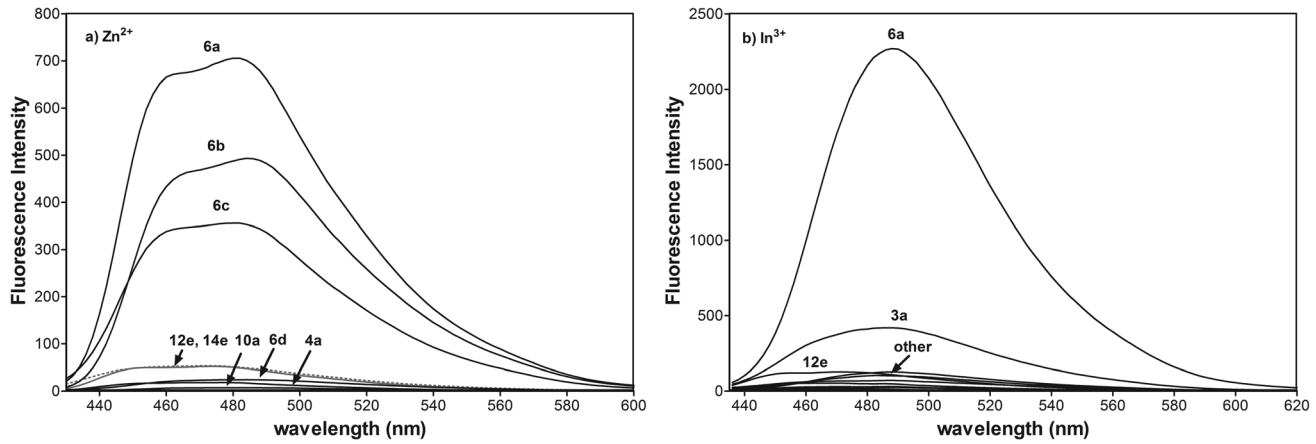

Fig. 4 (a) Fluorescence spectra of **4a**, **6a–d**, **10a**, **12e**, and **14e** (10 μM) in CH_3CN with 1 equiv. of Zn^{2+} (λ_{ex} = 415 nm, voltage 400 V), (b) fluorescence spectra of **3a**, **6a**, **10a**, **12e**, and **14e** (10 μM) in CH_3CN with 1 equiv. of In^{3+} (λ_{ex} = 425 nm, voltage 550 V).

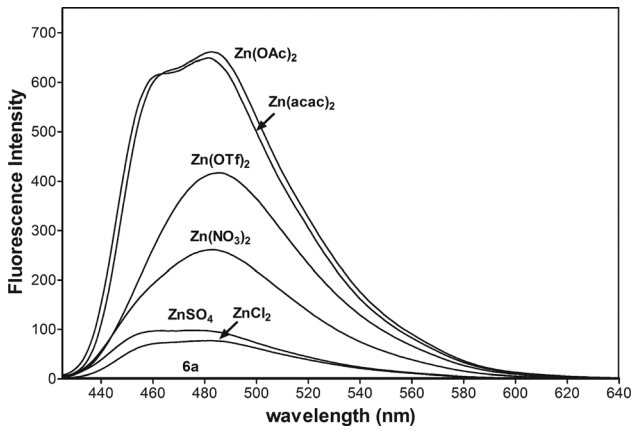

Fig. 5 Fluorescence spectra of **6a** (10 μM) in CH_3CN with 1 equiv. of $Zn(acac)_2$, $Zn(OAC)_2$, $Zn(OTf)_2$, $Zn(NO_3)_2$, $ZnSO_4$, and $ZnCl_2$ (λ_{ex} = 415 nm, voltage 400 V).

of the fluorophore. Furthermore, acetate and acetylacetonate anions may also interfere with the fluorescent probe, despite the fact that **6a-Zn(OAc)$_2$** and **6a-Zn(acac)$_2$** have similar fluorescent profiles to **6a-ZnCl$_2$**.

The basicity of anions should also affect the equilibrium of complex formation. The stronger bases such as acetate and acetylacetonate anions may more easily deprotonate the ligand **6a** than other weaker bases under study, especially the chloride anion, so the stronger bases should shift the equilibrium towards the formation of products. The fluorescence titration data confirmed that emissions for **6a-Zn** at λ_{ex} = 415 nm are saturated with 1.2 equiv. of $Zn(acac)_2$, 1.6 equiv. of $Zn(OAc)_2$, and 2.0 equiv. of $ZnCl_2$, respectively (Fig. 6a, ESI†).

As shown in Fig. 6b, UV-Vis spectra of **6a** exhibited two maximal absorptions at 385 and 403 nm. Upon addition of $Zn(OAc)_2$, the absorbance at these peaks decreased, whereas the new two absorption peaks appeared at 407 and 435 nm with an isosbestic point at 409 nm. The photometric titration for **6a-Zn** is saturated with 0.6 equiv. of Zn^{2+}.

To determine the binding stoichiometry of **6a** with $Zn(acac)_2$, the absorption of **6a** at 435 nm was plotted as a function of the molar fraction of **6a** under a constant total concentration of **6a** and Zn^{2+}. The resulting Job plot is shown in Fig. 6b. The maximum absorbance was reached when the molar fraction was 0.5, which indicates a 1 : 1 ratio for **6a-Zn**.

Published on 11 October 2013. Downloaded by Laurentian University on 04/11/2013 00:26:56.

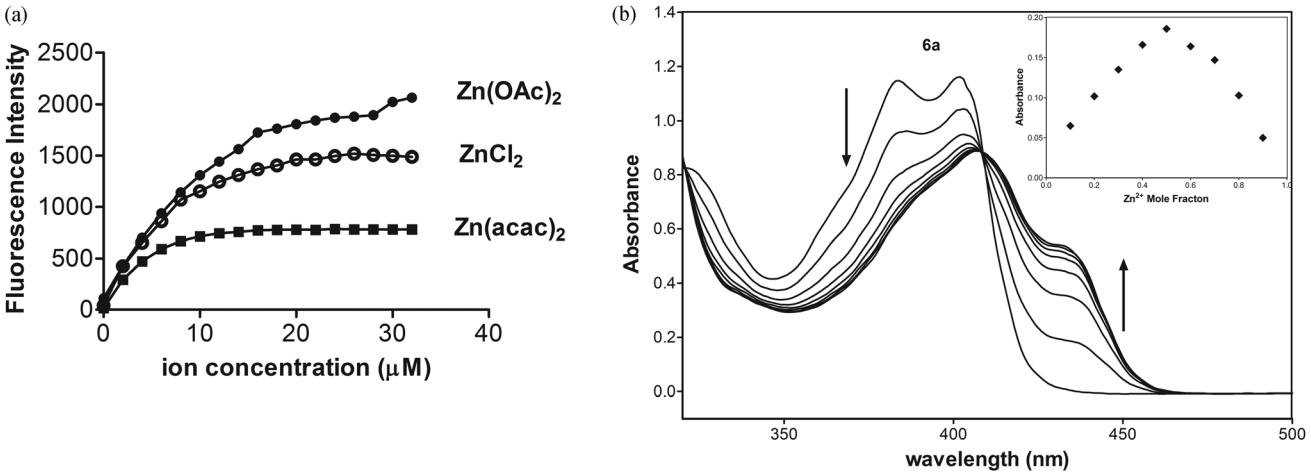

Fig. 6 (a) Increase in fluorescence intensity of **6a** (10 μM) in CH_3CN as the function of Zn^{2+} concentration for $Zn(acac)_2$ at $\lambda_{ex}/\lambda_{em}$ = 415/482 nm (400 V), $Zn(OAc)_2$ at $\lambda_{ex}/\lambda_{em}$ = 415/482 nm (450 V), and for $ZnCl_2$ $\lambda_{ex}/\lambda_{em}$ = 415/464 nm (550 V). (b) Absorption titration of **6a** (50 μM) in CH_3CN with 0.2 equiv. of $Zn(OAc)_2$. Inset: Job's plot for the binding of **6a** with $Zn(OAc)_2$ at λ = 435 nm in CH_3CN.

To evaluate the *E*/*Z* equilibrium during the formation of **6a**-Zn and confirm its binding mode, a detailed ^1H NMR titration was performed (Scheme 3, Fig. 7, ESI†). We used zinc acetylacetonate as a counter salt in ^1H NMR titration because the characteristic chemical shifts of the CH proton for the enol tautomer of acetylacetonate makes it possible to track the progress of complex formation.

Upon gradual addition of 0–0.6 equiv. of $Zn(acac)_2$ to a CD_3CN solution of (*E*/*Z*)-**6a**, a new set of signals were observed with the simultaneous reduction of the NH signal, indicating the formation of a complex. The protons (*E*/*Z*)-H-6 of the free ligand are upfield shifted from $\delta_{E\text{-H-6}}$ = 8.78 ppm and $\delta_{Z\text{-H-6}}$ = 8.62 ppm to δ = 8.40 ppm. Simultaneously, the protons (*E*)-H-8 and (*Z*)-H-8 are upfield and downfield shifted from $\delta_{E\text{-H-8}}$ = 8.11 ppm and $\delta_{Z\text{-H-8}}$ = 8.01 ppm to δ = 8.03 ppm, respectively (Fig. 7). These signals were attributed to the H-6 and H-8 of the complex. The CH and CH_2 protons of two tautomeric forms of acetylacetone also appeared at chemical shifts of δ = 5.63 and δ = 3.61 ppm, respectively. The presence of only one signal in the alkene region of the chemical shifts proved the formation of an L_2Zn complex with a 2 : 1 binding mode. Further addition of zinc ions from 0.6 to 1.4 equiv. revealed the reorganisation of the complex to **6a**-Zn-acac with a 1 : 1 binding mode of the ligand and zinc. This reorganisation was indicated by the appearance of the new set of broadened signals. In the diagnostic alkene region two additional signals appeared at δ = 5.67 and 5.45 ppm with the simultaneous increase of population of CH_2 for the keto form of acetylacetone relative to the populations of H-6 in the L_2Zn complex at 8.40 ppm and **6a**-Zn-acac at 8.49 ppm. The protons at 5.67 ppm and 5.45 ppm were attributed to the CH fragment of acetylacetone chelating the zinc in **6a**-Zn-acac and CH for zinc(II) acetylacetonate, respectively. The ^1H NMR study shows that the *Z* diastereoisomer of **6a** during the addition of zinc ion isomerises into its *E*-form, which coordinates the metal cation simultaneously with deprotonation. The upfield shifted signals for (*E*/*Z*)-H-6 reveal that the nitrogen atom at the N-5 position in pyrido[2,3-*b*]pyrrolo-[2,3-*e*]pyrazine derivatives **6a** does not directly coordinate the zinc cation during binding but probably facilitates the deprotonation and formation of complex (*E*)-**6**-Zn-acac.

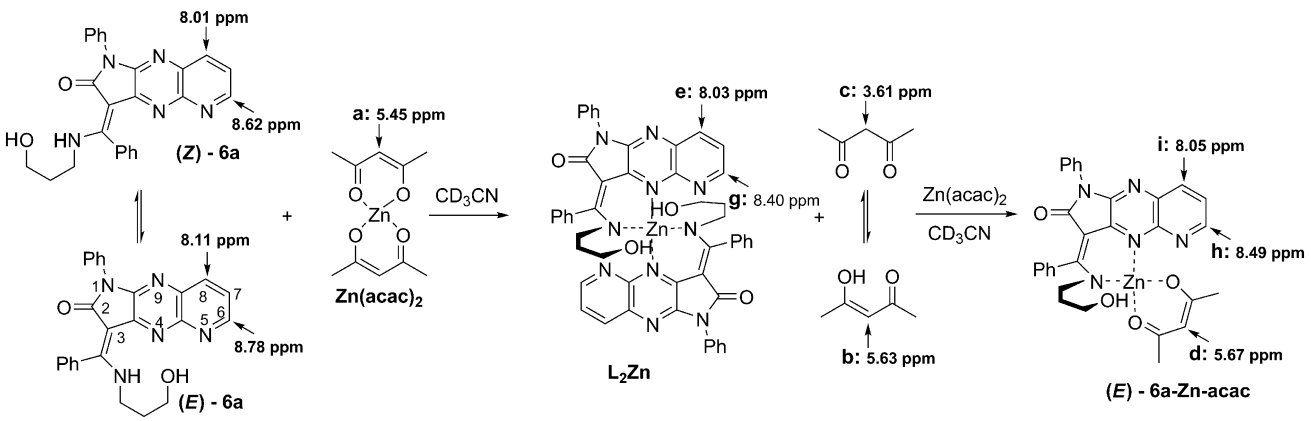

Scheme 3 Proposed binding modes of **6a** with $Zn(acac)_2$.

 This journal is © The Royal Society of Chemistry and the Centre National de la Recherche Scientifique 2013

Published on 11 October 2013. Downloaded by Laurentian University on 04/11/2013 00:26:56.

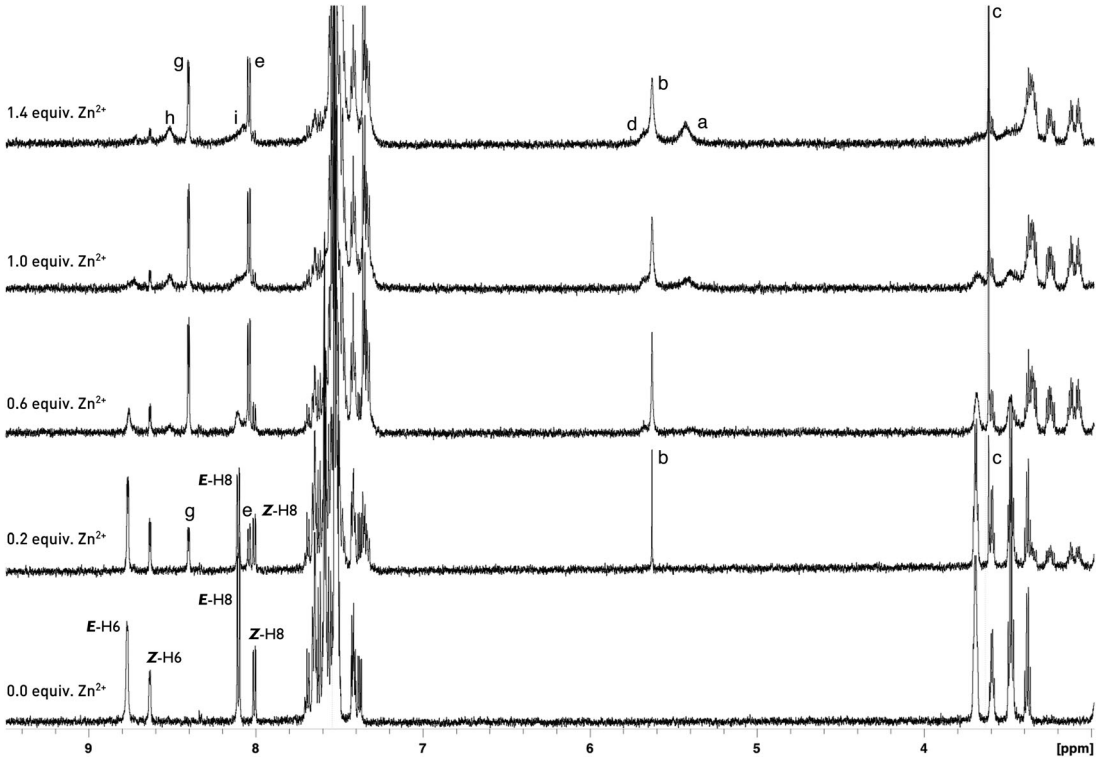

Fig. 7 Partial ^{1}H NMR spectra (600 MHz) of **6a** (5 mM) in the presence of different concentrations of $Zn(acac)_2$ in CD_3CN. (Please see the ESI† for partial ^{1}H NMR spectra of **6a** in the region 1–4 ppm.)

Reorganisation of the complex from L_2Zn to L-Zn-acac is not observed in fluorometric and photometric titrations. However, the ^{1}H NMR experiment indicated that two equilibria were estabilished during the formation of the complex with binding mode 1 : 1.

Quite different equilibria are revealed by ^{1}H NMR titration for *E*/*Z*-**6a** with $InCl_3$ (ref. 54 and 55) (Scheme 4, Fig. 8). After addition of 0.4 equiv. of indium ions probably two separate complexes with *E*- and *Z*-diastereisomers of **6a**, respectively, are formed. Interconversion of *Z*-**6a** to *E*-form and deprotonation during binding are not observed. Metal ions are consumed immediately and two sets of new signals appear indicating formation of the L_3M system. One set shows broadened signals for diagnostic protons H-6, H-7 and H-8, because of long range spin coupling of these protons with the ^{115}In isotope. These signals are shifted to 9.92, 8.55 and 8.43 ppm. Plausibly the indium ion binds to the N-5 nitrogen donor of the fluorophore. That coordination is possible for the *Z*-diastereoisomer of **6a** because the N-5 nitrogen atom is easily accessible. The *Z*-NH proton is upfield shifted and overlaps with the *E*-NH-form. The second set shows the three-spin system ABM with three different coupling constants $J_{H\text{-}6,H\text{-}7}$ = 4.9 Hz, $J_{H\text{-}7,H\text{-}8}$ = 8.1 Hz, and $J_{H\text{-}6,H\text{-}8}$ = 1.4 Hz. Protons H-6, H-7, and H-8 are upfield shifted to 8.95, 8.76, and 7.98 ppm, respectively. After addition of 0.6 equiv. of salt the new equilibria start to establish with two

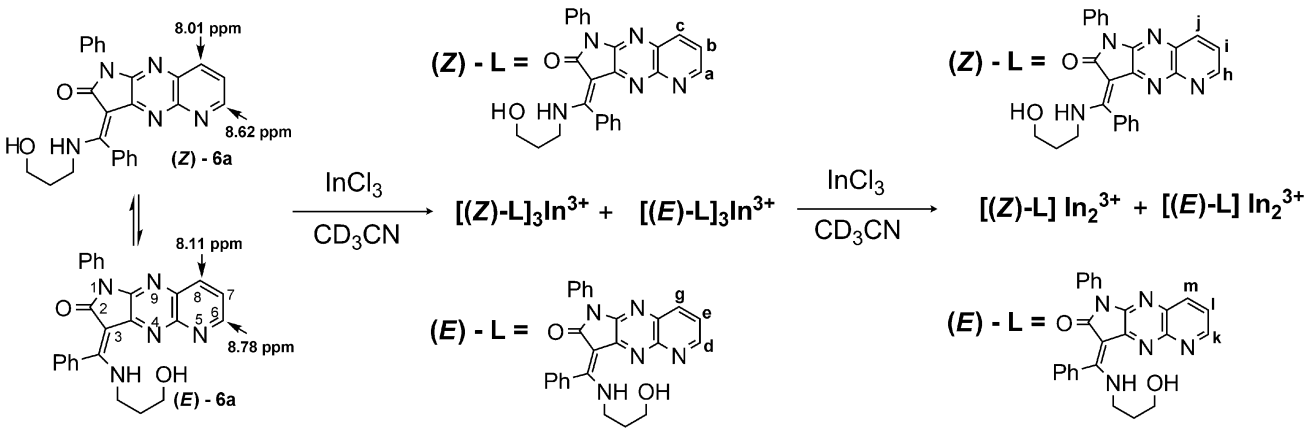

Scheme 4 Proposed binding modes of **6a** with $InCl_3$.

Published on 11 October 2013. Downloaded by Laurentian University on 04/11/2013 00:26:56.

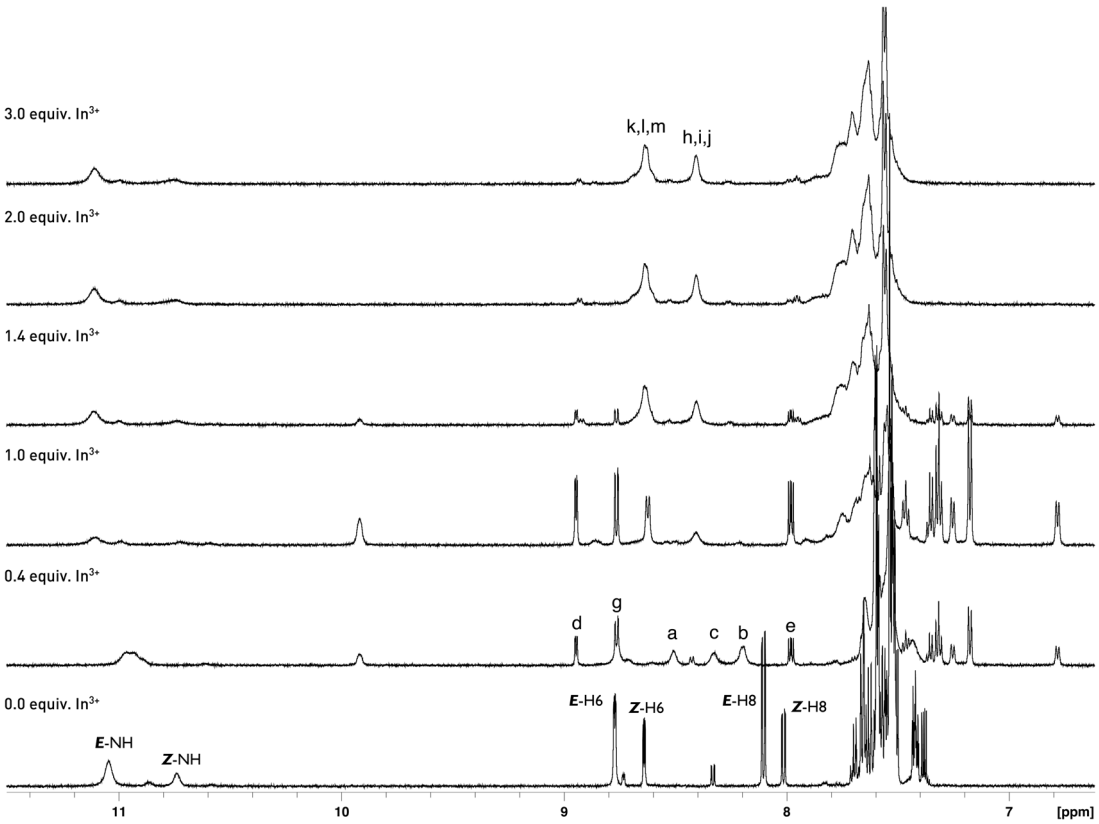

Fig. 8 Partial ^{1}H NMR spectra (600 MHz) of **6a** (5 mM) in the presence of different concentrations of $InCl_3$ in CD_3CN.

broadened set of signals in the ratio 2 : 1 indicating reorganisation and formation of the two new complexes with two N–H signals. Probably, two indium ions prefer binding to *E*/*Z*-**6a** at N-5 and N-9 nitrogen donors and form *E*-**6a-In$_2$** and *Z*-**6a-In$_2$**. All attempts to isolate these complexes failed.

As shown in Fig. 9a, upon addition of $InCl_3$ to **6a**, the absorbance decreased and the new broaden absorption peak appeared at 427 nm with an isosbestic point at 408 nm. The spectral change for **6a-In** terminates by the addition of 2 equiv. of In^{3+}. The fluorescence titration data show that emissions for **6a-In** at λ_{ex} = 425 nm appear after addition of 0.6 equiv. of metal ions and they are saturated with 3 equiv. of $InCl_3$ (Fig. 9b). This indicates that **6a** coordinates first with In^{3+}, producing non-emissive complexes. Further addition of these ions leads to the formation of emissive complexes.

The metal ions except gallium and thallium affect the absorption spectral profile of **6a** indicating the coordination of the ligand with Zn^{2+}, Cd^{2+}, Hg^{2+}, and In^{3+} ions (Fig. 10a).

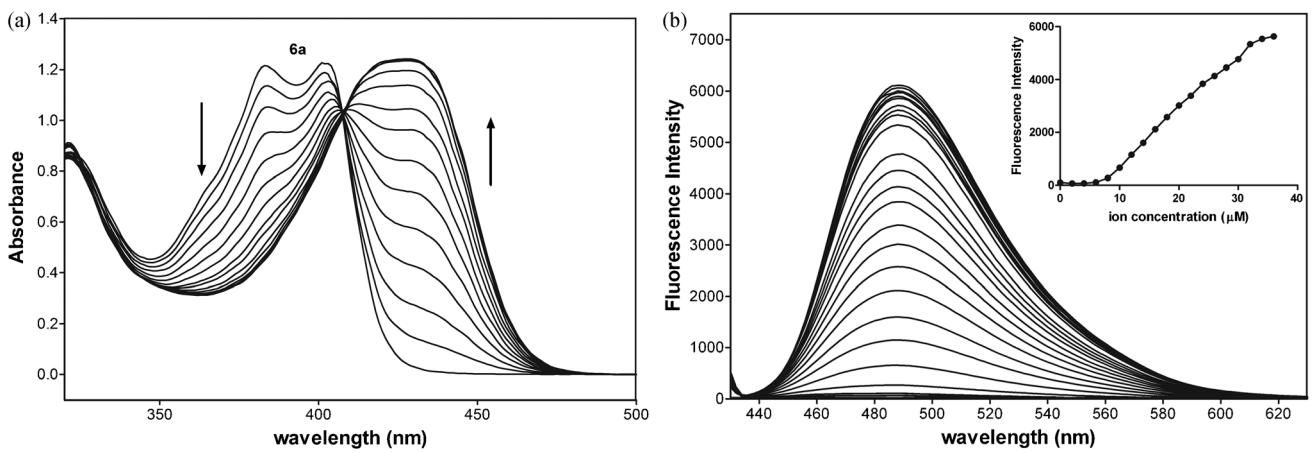

Fig. 9 (a) Absorption titration of **6a** (50 μM) in CH_3CN with 0.2 equiv. of $InCl_3$. (b) Fluorescence titration (λ_{ex} = 425 nm) of **6a** (10 μM) in CH_3CN with $InCl_3$. The concentration of In^{3+} was increased from 0 to 36 μM. Inset: increase in fluorescence intensity at λ_{em} = 488 nm as a function of In^{3+} concentration.

 This journal is © The Royal Society of Chemistry and the Centre National de la Recherche Scientifique 2013

Published on 11 October 2013. Downloaded by Laurentian University on 04/11/2013 00:26:56.

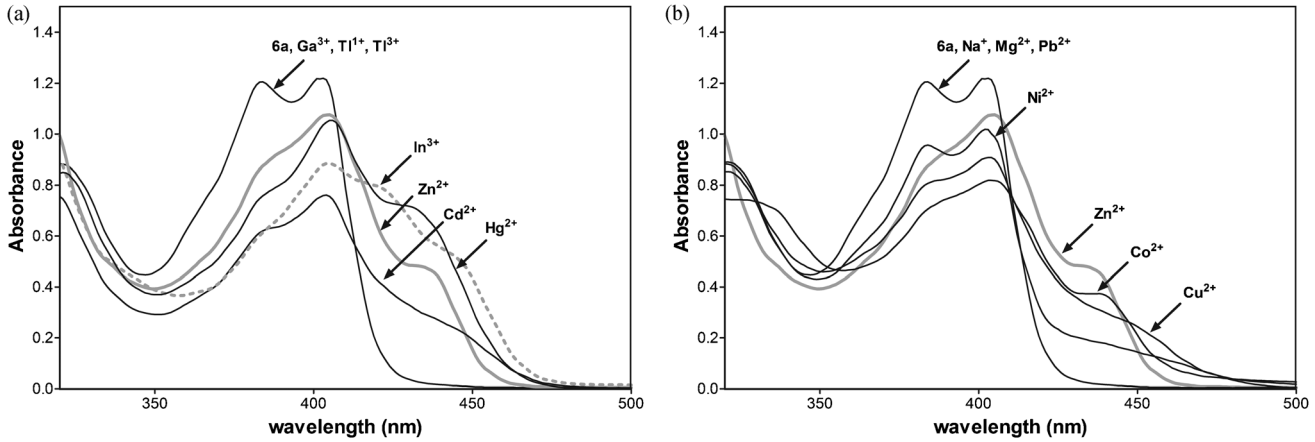

Fig. 10 (a) Absorption spectra of **6a** (50 μM) in CH_3CN with 1 equiv. of Zn^{2+}, Cd^{2+}, Hg^{2+}, Ga^{3+}, In^{3+}, Tl^{3+} and Tl^{1+}. (b) Absorption spectra of **6a** (50 μM) in CH_3CN with 1 equiv. of Zn^{2+}, Na^{+}, Mg^{2+}, Pb^{2+}, Ni^{2+}, Co^{2+} and Cu^{2+}.

The selectivity of **6a** towards Zn^{2+} and other metal ions was examined, and the results are shown in Fig. 11. An extremely low fluorescence emission intensity relative to that for Zn^{2+} was observed upon the addition of Cd^{2+}, Co^{2+}, Hg^{2+}, Mg^{2+}, Na^{+}, Ni^{2+}, and Pb^{2+} metal cations.

To study the influence of other metal ions on the binding of Zn^{2+} to **6a**, we performed competitive experiments between Zn^{2+} (10 μM) and Cd^{2+}, Cu^{2+}, Co^{2+}, Hg^{2+}, Mg^{2+}, Na^{+}, Ni^{2+} Pb^{2+}, and In^{3+} (10 μM, Fig. 11a and b). The addition of Hg^{2+}, Na^{+}, and Pb^{2+} have a negligible effect on Zn^{2+} sensing. The fluorescence of **6a** with Zn^{2+} is slightly quenched by Co^{2+}, Cd^{2+}, and Hg^{2+} ions. The great impact on the fluorescence emission of **6a** with Zn^{2+} has the presence of one equiv. of indium ions, quenching the emission. Three equiv. of In^{3+} enhance the fluorescence emission with the changes in the profile similar to **6a-In** indicating the displacement of zinc by the indium metal ion.

Additionally, the absorption data detected for **6a** and the metal ions (Fig. 10b) show that the addition of Na^{+}, Mg^{2+}, and Pb^{2+} does not affect the absorption spectral profile of **6a**. Thus, these metal cations most likely do not bind to the receptor and do not compete in complexation with **6a**. The most significant changes, indicating chelation, are observed upon the addition of Zn^{2+}, Cd^{2+}, Co^{2+}, Cu^{2+}, $Hg^{2+}$and Ni^{2+} metal ions. The addition of 1 equiv. of Cd^{2+}, Co^{2+}, or Hg^{2+} into the complex **6a** with Zn^{2+} slightly reduces the emission peak at 480 nm, indicating that the displacement of Zn^{2+} from the complex by Cd^{2+}, Co^{2+}, or Hg^{2+} ions is unfavourable. The competition experiment shows excellent selectivity for Zn^{2+} over all metal ions under study except In^{3+}.

The fluorescence properties of the new complexes are solvent-dependent, and the new complexes are non-fluorescent in the presence of water and in DMSO. To understand this phenomenon, we measured the ^1H NMR spectra of **6a** with 0.5, 1.0, 1.5, and 2.0 equiv. of $Zn(acac)_2$ in DMSO-d_6. All spectra, even that for the highest zinc cation concentration, show four sets of signals: *E*-, *Z*-diastereoisomers of **6a** with *E*/*Z*-NH signals and 2 : 1 and 1 : 1 complexes of **6a**-Zn. This polar aprotic solvent enhances solvation by hindering the deprotonation of the enamino group and thus the further formation of the complex (ESI†).

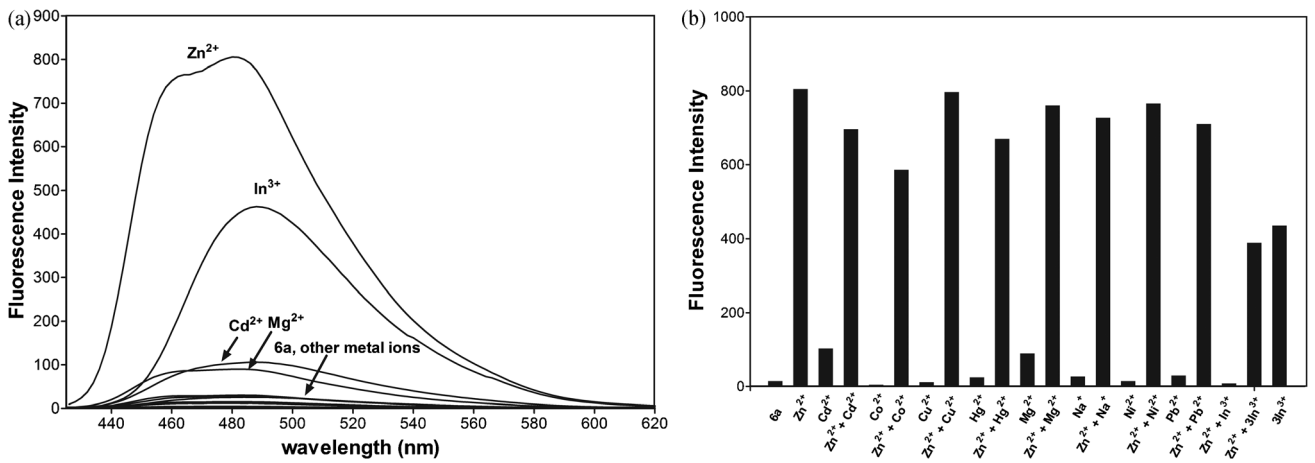

Fig. 11 (a) Fluorescence spectra of **6a** (10 μM) in CH_3CN with 1 equiv. of Cd^{2+}, Co^{2+}, Hg^{2+}, Mg^{2+}, Na^{+}, Ni^{2+}, Pb^{2+}, Zn^{2+}, and 3 equiv. of In^{3+} (λ_{ex} = 415 nm). (b) Metal ion selectivity profiles of **6a** (10 μM) in CH_3CN in the presence of various metal ions (10 μM) at $\lambda_{ex}/\lambda_{em}$ = 415/480 nm.

Published on 11 October 2013. Downloaded by Laurentian University on 04/11/2013 00:26:56.

Conclusions

We have designed and verified the sensing abilities of integrated azaheteroarene fluorophores, such as *N*-aryl or *N*-alkyl pyrido[2,3-*b*]pyrrolo[2,3-*e*]pyrazine (**6**), pyrido[2,3-*b*]pyrrolo[3,2-*e*]-pyrazine (**10**), pyrido-[3,4-*b*]pyrrolo[3,2-*e*]pyrazine (**12**), and pyrrolo[2,3-*b*]quinoxaline-7-carboxylic acid (**14**), integrated with 3-aminopropan-1-ol upon complexation with Zn^{2+}, Cd^{2+}, Hg^{2+}, Ga^{3+}, In^{3+}, and Tl^{3+} metal ions. We have shown that the [*N*, *N*, *O*] tridentate ligands **6a**, **6b**, and **6c** with the nitrogen atom at N-5 and *N*-aryl groups selectively respond to zinc and **6a** to indium ions in acetonitrile. The benzyl and (4-ethoxy)phenyl groups at the N-1 position weaken the acceptor character of the amide carbonyl group in fluoroionophore systems and quench ICT fluorescence enhancement for **6d**, **12e**, and **14e**. An additional nitrogen donor at N-7 or N-8 changes the electron density in ICT azaheteroarene indicators and that should also influence the dipole moment of fluorophores. Pyrido[2,3-*b*]pyrrolo[3,2-*e*]-pyrazine derivative **10a** with the nitrogen atom at N-8 does not exhibit fluorescence emission with Zn^{2+}, Cd^{2+}, Hg^{2+}, Ga^{3+}, In^{3+}, and Tl^{3+} metal ions. ^{1}H NMR titration showed two different mechanisms of binding Zn^{2+} and In^{3+} to **6a**. The *Z*-diastereoisomer of **6a** during the addition of the zinc ion isomerises to its *E*-form, which coordinates metal cations simultaneously with deprotonation in acetonitrile. Indium ions form two separate complexes with (*E*)-**6a** and (*Z*)-**6a** without deprotonation. Although ligands under study do not operate in aqueous media, further functionalisation of the receptor unit will allow us to obtain sensors with desirable physicochemical properties which will be reported in due course.

Experimental

Materials and instrumentation

All of the solvents for the UV and fluorescence spectra were obtained from Sigma-Aldrich or Merck and were of spectroscopic purity. The solution metal ions were prepared from $ZnCl_2$, $ZnSO_4$, $Zn(NO_3)_2$, $Zn(OTf)_2$, $Zn(acac)_2$, $Zn(OAc)_2$, $Ga(acac)_3$, $InCl_3$, $TlNO_3$, $Tl(OAc)_3$, $Cu(acac)_2$, $Ni(acac)_2$, $Co(acac)_2$, $Cd(acac)_2$, $Hg(OAc)_2$, NaOAc, $Pb(OAc)_2$, $Mg(OAc)_2$. Melting points were determined on a Boetius PHMK 05 melting point apparatus. IR spectra were measured on a Thermo Scientific Nicolet IR200 FT-IR. The ^{1}H NMR and ^{13}C NMR spectra were recorded using Bruker Avance III 600 and II 300 spectrometers at 300 K. The chemical shifts (δ) are reported in parts per million (ppm) on a δ scale downfield from TMS. The ^{1}H NMR spectra were referenced internally to the residual proton resonance in $CDCl_3$ (δ 7.26 ppm), DMSO-d_6 (δ 2.49 ppm), and CD_3CN (δ 1.96 ppm). The ^{13}C NMR spectra were referenced to $CDCl_3$ (δ 77.0 ppm), or, DMSO-d_6 (δ 39.7 ppm). The coupling constants (J) are reported in Hertz (Hz). Mass spectra were recorded on a Finnigan Mat 95 (EI, 70 eV) and ESI spectrometers. Microanalyses were performed with a Vario Micro Tube CHNS; the results agreed with the calculated values.

For the determination of ε and quantum yields indicated in Table 2, the analysed compounds were diluted in selected solvents to prepare 20 μM stock solutions: chloroform for **5** and **6** and acetonitrile for **9a**, **10a**, **12e**, **12f**, **14e**, and **14f** using a 1 mM stock solution prepared in DMSO. The fluorescence lifetimes were determined using a 20 μM stock solution in chloroform. The absorption spectra of compounds **5**, **6**, **9a**, **10a**, **12e**, **12f**, **14e**, and **14f** (Table 2) were recorded on a Microplate Reader Infinite M200 (Tekan) spectrophotometer in 1 cm cells at 25 °C.

The fluorescence measurements for all analysed compounds were done using a Hitachi F-4500 spectrofluorometer. All spectra were recorded at 25 °C with an excitation slit width of 5 nm, an emission slit of 10 nm and a PMT voltage of 700 V.

The fluorescence quantum yields of the analysed compounds were determined using 9,10-diphenylanthracene (Φ_s = 0.90 in cyclohexane) as a standard. The fluorescence lifetimes were determined using a time-correlated single-photon counting system based on the Horiba Jobin Yvon IBH lifetime spectrofluorometer system components, which consisted of a picosecond single-photon-detection TBX-04 module integrated with a fast photomultiplier, high-voltage power supply, GHz preamplifier and picosecond-timing discriminator. A picosecond pulsed laser diode (NanoLED-11, Horiba Jobin, Yvon) was used as a light source. The specimens were excited at 372 nm with a 1 MHz repetition rate. The fluorescence decays were observed through a cut-off filter of 475 nm (Andover Corporation Optical Filter). To avoid pulse pile-up, the power of the diode was adjusted to an appropriately low level using a neutral gradient filter. The excitation pulse diode laser profile, required for the deconvolution analysis, was measured using a diluted glycogen suspension without a filter. For the data acquisition and decay analysis, the Jobin Yvon IBH data station and DAS6 software were used. All measurements were performed at 25 °C, and each recorded lifetime was averaged from five independent decay measurements.

The Job plots for **6a** with $Zn(acac)_2$ and absorption spectra of **6a** (50 μM) in CH_3CN with respective 1 equiv. of metal cations were recorded on a Hitachi U-3900H spectrophotometer. The fluorescence measurements (Fig. 4, 5, 6a, 9b, 11a and b) were also recorded using a F-7000 FL spectrophotometer (25 °C, excitation and emission slit width of 5 nm, 400 V and 550 of PMT voltage). The fluorescence spectra were obtained using a 1 mM stock solution prepared in DMSO for compounds **4a**, **10a**, **12e**, and **14e**.

Substrates **5a–d**, **7a**, **11e,f**, and **13e,f** were synthesised according to previously reported procedures.[35,36]

X-ray structure analysis of 6a and 12e

Crystals of **6a** were obtained from acetonitrile solution by slow evaporation of the solvent under ambient conditions. The crystal suitable for X-ray diffraction experiment was a yellow plate of dimensions: 0.3 × 0.1 × 0.03 mm. X-ray diffraction data were collected at 130 K using a Nonius Brucker KappaCCD diffractometer with MoKα radiation (λ = 0.71073 Å), with the software Collect.[41] Data were processed using *HKL SCALEPACK*[42] and *HKL DENZO*.[42] The phase problem was solved by direct methods using SHELXS-97[43] program. The model parameters were refined by full-matrix least-squares

 This journal is © The Royal Society of Chemistry and the Centre National de la Recherche Scientifique 2013

Published on 11 October 2013. Downloaded by Laurentian University on 04/11/2013 00:26:56.

on F^2 using SHELXL-97.[43] All non-hydrogen atoms were refined anisotropically. H atoms attached to N and O atoms were located on the difference Fourier map. These in the hydroxyl group and the water molecule were refined using the DFIX restraint with a target bond length of 0.82 Å, within an assumed estimated standard deviation of 0.02 Å. For the water molecule the DANG restraint was applied with an H1w···H2w distance of 1.35 Å, within an assumed estimated standard deviation of 0.04 Å. Positions of hydrogen atoms attached to C atoms were calculated with C–H = 0.95 Å for aromatic, C–H = 0.99 Å for methylene and were refined using the riding model with the isotropic displacement parameter U_{iso} = 1.2 U_{eq} of the parent atom. Crystal data: moiety formula $C_{25}H_{21}N_5O_2\ H_2O$, M_r = 441.48, monoclinic, space group $P2_1/c$, a = 11.2202(2) Å, b = 6.1966(4) Å, c = 31.8009(10) Å, β = 109.409(2)°, V = 2085.48(15) Å^3, Z = 4, D_c = 1.406 g cm^{-3}, μ(MoKα) = 0.10 mm^{-1}, F(000) = 928; 14 239 collected reflections, 4696 unique (R_{int} = 0.057), 3177 observed ($I > 2\sigma(I)$). For 313 refined parameters, the final R_1 = 0.062 for reflections with $F^2 > 2\sigma(F^2)$, wR_2 = 0.186 for all unique reflections, S = 1.04.

Crystals of **12e** were obtained from DMSO-d_6 solution by slow evaporation of the solvent under ambient conditions. The crystal suitable for X-ray diffraction experiment was a yellow prism of dimensions: 0.45 × 0.3 × 0.3 mm. X-ray diffraction data were collected at 110 K using a SuperNova diffractometer with MoKα radiation (λ = 0.71073 Å). Data were processed using *CRYSALIS^{Pro}*.[44] The phase problem was solved using direct methods with SHELXS-97[43] program. The model parameters were refined by full-matrix least-squares on F^2 using SHELXL-97.[43] All non-hydrogen atoms were refined anisotropically. H atoms attached to N and O atoms were located on the difference Fourier map and refined independently. Positions of hydrogen atoms attached to C atoms were calculated with C–H = 0.95 Å for aromatic, C–H = 0.99 Å for methylene and were refined using the riding model with the isotropic displacement parameter U_{iso} = 1.2 U_{eq} of the parent atom. Crystal data: moiety formula $C_{26}H_{23}N_5O_2$, M_r = 437.49, monoclinic, space group $P2_1/c$, a = 9.1766(1) Å, b = 11.1148(1) Å, c = 21.7846(2) Å, β = 106.341(1)°, V = 2132.19(4) Å^3, Z = 4, D_c = 1.363 g cm^{-3}, μ(MoKα) = 0.09 mm^{-1}, F(000) = 920; 32 725 collected reflections, 5395 unique (R_{int} = 0.032), 4494 observed ($I > 2\sigma(I)$). For 323 refined parameters, the final R_1 = 0.039 for reflections with $F^2 > 2\sigma(F^2)$, wR_2 = 0.103 for all unique reflections, S = 1.03.

WinGX[45] software was used to prepare materials for publication. Figures showing asymmetric units of **6a** and **12e** were made using ORTEP-3 for Windows.[46] For calculation of the weighted least-squares planes through selected atoms program PARST[47,48] was used. Crystallographic data (excluding structure factors) for the structures in this paper have been deposited with the Cambridge Crystallographic Data Centre as supplementary publication nos. CCDC 890197 and 890198 for structure of **12e** and **6a**, respectively.

General procedure: synthesis of enaminone 6a–d, 10a, 12e, 12f, 14e, and 14f

A benzoyl-azaheteroarene derivative **5**, **9**, **11**, or **13** (0.55 mmol) was added to the amine (2 mL). The mixture was left for 5 days, and then diluted with cold H_2O (100 mL). The precipitated solid was collected by filtration, washed with H_2O, and crystallised from acetonitrile.

(*E*/*Z*)-3-[(3-Hydroxypropylamino)-phenylmethylidene]-1,3-dihydro-2*H*-1-phenylpyrido[2,3-*b*]pyrrolo[2,3-*e*]pyrazin-2-one 6a. Yellow needles (228 mg, 98%), m.p. 198 °C. *E*/*Z* = 10 : 1 ($CDCl_3$), *E*/*Z* = 2.7 : 1 (DMSO-d_6), *E*/*Z* = 2.6 : 1 (CD_3CN). IR (ATR): 3335, 3207, 3070, 2927, 2875, 1704, 1596 cm^{-1}. ^{1}H NMR (300.13 MHz, DMSO-d_6): δ = 1.69 (quint, 2H, J = 6.0 Hz, *Z*-CH_2), 1.76 (quint, 2H, J = 6.0 Hz, *E*-CH_2), 3.31 (s, H_2O) 3.41 (m, 6H, *E*/*Z*-CH_2NH, *Z*-CH_2OH), 3.54 (q, 2H, J = 6.0 Hz, *E*-CH_2OH), 4.62 (t, 2H, J = 6.0. Hz, *E*/*Z*-OH), 7.37–7.62 (m, 22H, *E*/*Z*-H-Ar), 8.04 (d, J = 8.2 Hz, *Z*-H-8), 8.14 (dd, 1H, J = 1.8 Hz, J = 8.2 Hz, *E*-H-8), 8.58 (d, 1H, J = 4.3 Hz, *Z*-H-6), 8.74 (dd, 1H, J = 1.8 Hz, J = 4.3 Hz, *E*-H-6), 10.69 (br. s, 1H, *Z*-NH), 10.89 (br. s, 1H, *E*-NH). ^{13}C NMR (75.47 MHz, DMSO-d_6): δ = 32.91, 42.05, 57.85, 89.49, 122.29, 127.39, 127.49, 128.01, 128.54, 128.80, 130.15, 130.52, 133.53, 136.03, 148.29, 165.17, 166.48, 173.50. MS-ESI: m/z 424 (M^+ + 1). Anal. calcd for $C_{25}H_{21}N_5O_2$ + H_2O: C, 68.01; H, 5.25; N, 15.86%. Found: C, 67.99; H, 4.95; N, 15.71%.

(*E*/*Z*)-1-(4-Chlorophenyl)-3-[(3-hydroxypropylamino)-phenylmethylidene]-1,3-dihydro-2*H*-pyrido-[2,3-*b*]pyrrolo[2,3-*e*]pyrazin-2-one 6b. Yellow needles (246 mg, 98%), m.p. 175 °C. *E*/*Z* = 8.7 : 1 ($CDCl_3$), *E*/*Z* = 3.2 : 1 (DMSO-d_6). IR (ATR): 3331, 3207, 3062, 2957, 2923, 1702, 1593 cm^{-1}; ^{1}H NMR (300.13 MHz, DMSO-d_6); δ = 1.69 (quint, 2H, *Z*-CH_2), 1.75 (quint, 2H, J = 6.3 Hz, *E*-CH_2), 3.43 (m, 4H, *E*/*Z*-CH_2NH_2), 3.56 (m, 4H, *E*/*Z*-CH_2OH), 4.35 (t, 1H, *E*-OH), 4.62 (t, 1H, *Z*-OH), 7.37–7.70 (m, 20H, *E*/*Z*-H-Ar), 8.03 (1H, d, J = 8.1 Hz, *Z*-H-8), 8.05 (1H, dd, J = 8.0 Hz, J = 1.7 Hz, *E*-H-8), 8.58 (1H, dd, J = 4.5 Hz, J = 1.7 Hz, *Z*-H-6), 8.75 (1H, dd, J = 4.5 Hz, J = 1.7 Hz, *E*-H-6), 10.69 (br. s, 1H, *Z*-NH), 10.89 (br. s, 1H, *E*-NH). ^{13}C NMR (75.47 MHz, DMSO-d_6) δ = 32.88, 42.10, 57.85, 89.41, 122.34, 128.01, 128.56, 128.79, 128.90, 130.20, 130.45, 131.70, 132.42, 133.30, 136.04, 146.45, 148.19, 148.44, 164.93, 166.54. MS-ESI: m/z 458 (M^+ + 1). Anal. calcd for $C_{25}H_{20}ClN_5O_2$ + H_2O: C, 63.09; H, 4.66; N, 14.71%. Found: C, 63.17; H, 4.46; N, 14.85%.

(*E*/Z)-1-(4-Methylphenyl)-3-[(3-hydroxypropylamino)-phenylmethylidene]-1,3-dihydro-2*H*-pyrido-[2,3-*b*]pyrrolo[2,3-*e*]pyrazin-2-one 1-aminopropanol hydrate 6c. Yellow needles (198 mg, 83%), m.p. 198 °C. *E*/*Z* = 8.7 : 1 ($CDCl_3$), *E*/*Z* = 3 : 1 (DMSO-d_6). IR (ATR): 3435, 3282, 3040, 2925, 2890, 1709, 1607 cm^{-1}. ^{1}H NMR (300.13 MHz, $CDCl_3$) for crude product **6c** + $NH_2(CH_2)_3OH$, H_2O: δ = 1.62 (m, 2H, J = 5.8 Hz, CH_2), 1.90 (m, 4H, J = 5.8 Hz, *E*/*Z*-CH_2), 2.36 (s, 3H, *E*-CH_3), 2.44 (s, 3H, *Z*-CH_3), 2.63 (br. s, 4H, *E*/*Z*-OH, H_2O) 2.97 (t, 2H, J = 5.8 Hz, CH_2NH_2), 3.44 (br. m, 2H, *Z*-CH_2NH), 3.56 (t, 2H, J = 5.8 Hz, *E*-CH_2NH), 3.78–3.88 (m, 6H, J = 5.8 Hz, *E*/*Z*-CH_2-OH; CH_2OH), 7.23–7.66 (m, 20H, *E*/*Z*-H-Ar), 8.09 (dd, 1H, J = 1.8 Hz, J = 8.1 Hz, *Z*-H-5), 8.19 (dd, 1H, J = 1.8 Hz, J = 8.1 Hz, *E*-H-7), 8.69 (dd, 2H, J = 4.4 Hz, J = 1.8 Hz, *E*/*Z*-H-6), 10.77 (br. s, 1H, *Z*-NH), 11.09 (br. s, 1H, *E*-NH). ^{13}C NMR (75.47 MHz, $CDCl_3$) for crude product **6c** + $NH_2(CH_2)_3OH$, H_2O: δ = 21.17, 32.53, 33.73, 41.43, 42.29, 59.12, 63.41, 90.27, 121.78, 126.59, 127.56, 128.74, 129.43, 130.25, 130.44, 134.15, 136.91, 137.34, 147.28, 147.68, 148.54, 149.25, 166.14, 166.78. ^{1}H NMR (300.13 MHz, DMSO-d_6) **6c**: δ = 1.69 (quint, 2H,

Published on 11 October 2013. Downloaded by Laurentian University on 04/11/2013 00:26:56.

J = 6.0 Hz, Z-CH_2), 1.76 (quint, 2H, J = 6.0 Hz, E-CH_2), 2.36 (s, 3H, E-CH_3), 2.44 (s, 3H, Z-CH_3), 2.63 (br. s, 4H, E/Z-OH, H_2O) 2.97 (t, 2H, J = 5.8 Hz, CH_2NH_2), 3.44 (br. m, 2H, Z-CH_2NH), 3.56 (t, 2H, J = 5.8 Hz, E-CH_2NH), 3.78–3.89 (m, 6H, J = 5.8 Hz, E/Z-CH_2-OH; CH_2OH), 7.23–7.66 (m, 20H, E/Z-H-Ar), 8.09 (dd, 1H, J = 1.8 Hz, J = 8.1 Hz, Z-H-5), 8.19 (dd, 1H, J = 1.8 Hz, J = 8.1 Hz, E-H-7), 8.69 (dd, 2H, J = 4.4 Hz, J = 1.8 Hz, E/Z-H-6), 10.58 (br. s, 1H, Z-NH), 11.09 (br. s, 1H, E-NH). MS-ESI: m/z 438 (M^+ + 1). Anal. calcd for $C_{26}H_{23}N_5O_2 + H_2O$: C, 68.56; H, 5.53; N, 15.37%. Found: C, 68.93; H, 5.28; N, 14.90%.

(*E*/*Z*)-1-(4-Ethoxyphenyl)-3-[(3-hydroxypropylamino)-phenylmethylidene]-1,3-dihydro-2*H*-pyrido-[2,3-*b*]pyrrolo[2,3-*e*]pyrazin-2-one 6d. Yellow needles (130 mg, 51%), m.p. 208–209 °C. E/Z = 7.1 : 1 ($CDCl_3$), E/Z = 2.9 : 1 (DMSO-d_6). IR (ATR): 3445, 3275, 3076, 2978, 2937, 1714, 1642 cm^{-1}. ^1H NMR (300.13 MHz, $CDCl_3$) for crude product **6d**: δ = 1.37–1.48 (m, 6H, J = 6.0 Hz, E/Z-CH_3), 1.85–1.97 (m, 4H, J = 6.0 Hz, E/Z-CH_2), 3.46 (q, 2H, J = 6.0 Hz, Z-CH_2NH), 3.56 (q, 2H, J = 6.0 Hz, E-CH_2NH), 3.80 (t, 2H, J = 5.8 Hz, Z-CH_2OH) 3.87 (t, 2H, J = 5.8 Hz, E-CH_2OH), 4.01–4.14 (m, 4H, J = 6.0 Hz, E/Z-CH_2O), 6.95 (d, 2H, J = 8.7 Hz, E-H-3′/5′), 7.07 (d, 2H, J = 8.7 Hz, Z-H-3′/5′) 7.38–7.65 (m, 20H, E/Z-H-Ar), 8.09 (dd, 1H, J = 1.9 Hz, J = 8.1 Hz, Z-H-5), 8.18 (dd, 1H, J = 1.8 Hz, J = 8.1 Hz, E-H-7), 8.70 (dd, 1H, J = 4.5 Hz, J = 1.8 Hz, E-H-6), 8.75 (dd, 1H, J = 4.4 Hz, J = 1.9 Hz, Z-H-6), 10.77 (br. s, 1H, Z-NH), 11.06 (br. s, 1H, E-NH). ^{13}C NMR (75.47 MHz, $CDCl_3$) for crude product **6d**: δ = 14.77, 32.61, 42.33, 59.25, 59.50, 63.65, 90.26, 114.75, 115.03, 121.79, 125.57, 127.57, 128.01, 128.73, 130.25, 130.41, 134.16, 136.81, 147.36, 147.77, 148.49, 149.27, 158.11, 166.28, 166.72. MS-ESI: m/z 468 (M^+ + 1). Anal. calcd for $C_{27}H_{25}N_5O_3$: C, 69.36; H, 5.39; N, 14.98%. Found: C, 69.13; H, 5.28; N, 14.90%.

(*E*/*Z*)-3-[(3-Hydroxypropylamino)-phenylmethylidene]-1,3-dihydro-2*H*-1-phenylpyrido[2,3-*b*]pyrrolo[3,2-*e*]pyrazin-2-one 10a. Yellow needles (175 mg, 75%), m.p. 266 °C. E/Z = 2 : 1 ($CDCl_3$), E/Z = 1.9 : 1 (DMSO-d_6). IR (ATR): 3235, 3059, 2862, 1711, 1609, 1587, 1561 cm^{-1}. ^1H NMR (300.13 MHz, $CDCl_3$): δ = 1.83 (m, 2H, Z-CH_2), 1.90 (m, 2H, E-CH_2), 2.05 (br. s, 2H, E/Z-OH), 3.43–3.54 (m, 4H, E/Z-CH_2NH), 3.77 (t, 2H, J = 5.8 Hz, Z-CH_2OH), 3.83 (t, 2H, J = 5.8 Hz, E-CH_2OH), 7.28–7.74 (m, 22H, E/Z-H-Ar), 8.16 (dd, 1H, J = 1.7 Hz, J = 8.1 Hz, E-H-5), 8.66 (dd, 1H, J = 1.7 Hz, J = 4.4 Hz, 1H, Z-H-7), 8.74 (dd, 1H, J = 1.7 Hz, J = 4.4 Hz, 1H, E-H-7), 10.59 (br. s, 1H, Z-NH), 10.74 (br. s, 1H, E-NH). ^{13}C NMR (75.47 MHz, $CDCl_3$): δ = 32.32, 32.62, 42.01, 59.77, 90.16, 121.58, 126.72, 127.19, 127.63, 128.02, 128.68, 128.76, 128.99, 130.30, 132.74, 133.90, 135.20, 137.02, 148.86, 161.07, 166.08. MS-ESI: m/z 423 (M^+ + 1). 424; anal. calcd for $C_{25}H_{21}N_5O_2 + H_2O$: C, 70.91; H, 5.0; N, 16.54%. Found: C, 70.92; H, 5.03; N, 16.29%.

(*E*/*Z*)-1-Benzyl-3-[(3-hydroxypropylamino)-phenylmethylidene]-1,3-dihydro-2*H*-pyrido[3,4-*b*]pyrrolo[3,2-*e*]pyrazin-2-one 12e. Yellow needles (85 mg, 35%), m.p. 221 °C. E/Z = 2.0 : 1 ($CDCl_3$), E/Z = 2.1 : 1 (DMSO-d_6). IR (ATR): 3411, 3241, 3060, 2937, 2870, 1703, 1612 cm^{-1}. ^1H NMR (300.13 MHz, $CDCl_3$): δ = 1.87 (m, 2H, J = 6.0 Hz, Z-CH_2), 1.92 (m, 2H, J = 6.0 Hz, E-CH_2; 2H, E/Z-OH), 3.46 (q, 2H, J = 6.0 Hz, Z-CH_2-NH), 3.51 (q, 2H, J = 6.0 Hz, E-CH_2-NH), 3.79 (t, 2H, J = 6.0 Hz, Z-CH_2-OH), 3.85 (t, 2H, J = 6.0 Hz, E-CH_2-OH), 5.05 (s, 2H, E-CH_2Bn), 5.23 (s, 2H, Z-CH_2Bn), 7.20–7.63 (m, 22H, E/Z-H-Ar), 8.36 (d, 1H, J = 5.6 Hz, Z-H-6), 8.52 (d, 1H, J = 5.6 Hz, E-H-6), 9.13 (s, 1H, Z-H-8), 9.20 (s, 1H, E-H-8), 10.61 (t, 1H, Z-NH), 10.78 (t, 1H, E-NH). ^{13}C NMR (75.47 MHz, $CDCl_3$): δ = 32.56, 41.94, 42.08, 59.75, 104.89, 119.99, 127.43, 127.59, 127.87, 128.41, 128.60, 128.69, 128.81, 130.25, 130.50, 136.98, 151.19, 166.33, 166.65. MS-ESI: m/z 438 (M^+ + 1). Anal. calcd for $C_{27}H_{25}N_5O_2 + H_2O$: C, 69.07; H, 5.80; N, 14.92%. Found: C, 68.77; H, 5.61; N, 14.73%.

(*E*/*Z*)-1-(2-Phenylethyl)-3-[(3-hydroxypropylamino)-phenylmethylidene]-1,3-dihydro-2*H*-pyrido[3,4-*b*]pyrrolo[3,2-*e*]pyrazin-2-one 12f. Yellow needles (52 mg, 21%), m.p. 145 °C. E/Z = 2.6 : 1 ($CDCl_3$), E/Z = 2.2 : 1 (DMSO-d_6). IR (ATR): 3414, 3056, 2944, 2826, 2748, 1697, 1609 cm^{-1}. ^1H NMR (300.13 MHz, $CDCl_3$): δ = 1.87 (quint, 2H, J = 6.0 Hz, Z-CH_2), 1.93 (quint, 2H, J = 6.0 Hz, E-CH_2; 2H, E/Z-OH; H_2O), 3.00–3.05 (m, 2H, E-CH_2Ph), 3.12–3.18 (m, 2H, Z-CH_2Ph), 3.47 (q, 2H, J = 6.0 Hz, Z-CH_2NH), 3.51 (q, 2H, J = 6.0 Hz, E-CH_2NH), 3.80 (t, 2H, J = 6.0 Hz, Z-CH_2-OH), 3.87 (t, 2H, J = 6.0 Hz, E-CH_2-OH), 4.07–4.12 (m, 2H, E-CH_2N), 4.25–4.31 (m, 2H, Z-CH_2N), 7.25–7.63 (m, 22 H, E/Z-H-Ar), 8.36 (d, 1H, J = 5.6 Hz, Z-H-6), 8.52 (d, 1H, J = 5.6 Hz, E-H-6), 9.13 (s, 1H, Z-H-8), 9.19 (s, 1H, E-H-8), 10.59 (t, 1H, Z-NH), 10.75 (t, 1H, E-NH). ^{13}C NMR (75.47 MHz, $CDCl_3$): δ = 32.31, 32.55, 34.25, 39.81, 42.10, 59.76, 90.94, 120.00, 126.35, 127.53, 127.92, 128.39, 128.48, 128.82, 128.94, 130.46, 138.56, 144.21, 149.14, 151.16, 166.49. MS-ESI: m/z 452 (M^+ + 1). Anal. calcd for $C_{27}H_{25}N_5O_2 + H_2O$: C, 69.07; H, 5.80; N, 14.92%. Found: C, 68.77; H, 5.61; N, 14.73%.

(*E*/*Z*)-1-Benzyl-3-[(3-hydroxypropylamino)-phenylmethylidene]-1,3-dihydro-2*H*-pyrrolo[2,3-*b*]quinoxaline-7-carboxylic acid 14e. Yellow needles (111 mg, 42%), m.p. 156 °C. E/Z = 2.2 : 1 (DMSO-d_6). IR (ATR): 3211, 3058, 3034, 2927, 2878, 1690, 1614, 1591, 1573 cm^{-1}. ^1H NMR (300.13 MHz, DMSO-d_6): δ = 1.71 (quint, 2H, J = 6.3 Hz, Z-CH_2), 1.77 (quint, 2H, J = 6.3 Hz, E-CH_2), 3.35–3.39 (m, 4H, Z/E-CH_2NH), 3.47 (t, 2H, Z-CH_2OH), 3.58 (t, 2H, E-CH_2OH), 4.65 (s, 1H, Z-OH), 4.76 (s, 1H, E-OH), 4.93 (s, 2H, E-CH_2Bn), 5.15 (s, 2H, Z-CH_2Bn), 7.18–7.65 (m, 21H, E/Z-H-Ar), 7.84 (dd, 1H, J = 8.5 Hz, J = 1.9 Hz, Z-H-7), 7.95 (d, 1H, J = 8.5 Hz, Z-H-8), 8.02 (dd, 1H, J = 8.5 Hz, J = 1.7 Hz, E-H-7), 8.25 (d, 1H, J = 1.9 Hz, Z-H-5), 8.31 (d, 1H, J = 1.7 Hz, E-H-5), 10.50 (t, 1H, J = 5.6 Hz, Z-NH), 10.75 (t, 1H, J = 5.6 Hz, E-NH), 13.00 (s, 2H, COOH). ^{13}C NMR (75.47 MHz, DMSO-d_6): δ = 32.31, 32.53, 41.28, 41.43, 42.25, 42.42, 58.27, 58.34, 89.44, 89.72, 125.60, 125.87, 127.30, 127.67, 127.85, 128.06, 128.21, 128.35, 128.53, 128.60, 129.13, 130.09, 130.21, 130.62, 130.94, 137.10, 137.33, 137.49, 137.69, 141.39, 142.14, 146.93, 147.00, 165.56, 165.61, 165.80, 167.23, 169.44. MS-ESI: m/z 481 (M^+). Anal. calcd for $C_{28}H_{25}N_4O_4$: C, 69.84; H, 5.23; N, 11.64%. Found: C, 69.85; H, 4.95; N, 11.62%.

1-Hydroxypropan-3-ammonium (*E*/*Z*)-1-(phenylethyl)-3-[(3-hydroxy-propylamino)-phenylmethylidene]-1,3-dihydro-2*H*-pyrrolo-[2,3-*b*]quinoxaline-7-carboxylate hydrate 14f. Yellow needles (100 mg, 31%), m.p. 107 °C. E/Z = 2.8 : 1 (DMSO-d_6). IR (ATR): 3350, 3210, 3031, 2928, 2870, 1672, 1585, 1557 cm^{-1}. ^1H NMR (300.13 MHz, DMSO-d_6) for **14f** + $NH_2(CH_3)_2OH$: δ = 1.73 (m, 6H, J = 6.85 Hz, CH_2, E/Z-CH_2), 2.87 (t, 4H, J = 7.04 Hz, E/Z-CH_2Ph),

This journal is © The Royal Society of Chemistry and the Centre National de la Recherche Scientifique 2013

Published on 11 October 2013. Downloaded by Laurentian University on 04/11/2013 00:26:56.

2.96 (t, 2H, J = 7.7 Hz, CH_2NH_2), 3.10 (t, 1H, J = 7.5 Hz, OH), 3.33 (m, 4H, *E*/*Z*-CH_2NH), 3.44–3.59 (m, 8H, *E*/*Z*-CH_2OH, *E*/*Z*-CH_2N), 3.39 (t, 2H, CH_2OH), 4.19 (t, 1H, *E*/*Z*-OH), 7.09–7.64 (m, 21H, *E*/*Z*-H-Ar), 7.82 (d, 1H, J = 8.5 Hz, *E*-H-8), 7.85 (dd, 1H, J = 1.9 Hz, *Z*-H-7), 8.02 (dd, 1H, J = 8.5 Hz, J = 1.7 Hz, *E*-H-7), 8.23 (d, 1H, J = 1.9 Hz, *Z*-H-5), 8.31 (d, 1H, J = 1.7 Hz, *E*-H-5), 10.36 (s, 1H, *Z*-NH), 10.58 (s, 1H, *E*-NH). ^{13}C NMR (75.47 MHz, DMSO-d_6): δ = 31.36, 32.44, 33.67, 36.79, 42.02, 58.24, 89.73, 125.97, 126.39, 126.76, 128.14, 128.52, 128.76, 129.92, 130.83, 136.95, 137.79, 138.80, 139.36, 145.71, 146.52, 164.59, 165.65, 169.32. MS-ESI: m/z 493 ($M^+ - 1$). Anal. calcd for $C_{32}H_{37}N_5O_6$ (**14f** + $NH_2(CH_3)_2OH$ + H_2O): C, 65.40; H, 6.35; N, 11.92%. Found: C, 65.46; H, 6.30; N, 11.89%.

General procedure: synthesis of 2*H*-pyrido[2,3-*b*]pyrrolo[3,2-*e*]-pyrazin-2-one 9

Triethylamine (172 mg, 0.23 mL, 2 mmol) was added to a solution of **7a** (498 mg, 1.7 mmol) in EtOH at rt. The mixture was stirred for 2 h and then EtOH was evaporated. The precipitate was dissolved in CH_2Cl_2 (30 mL). $SOCl_2$ (212 mg, 0.13 mL, 1.78 mmol) was added to an ice-cooled stirred CH_2Cl_2 solution at 0 °C. After 1 h, the mixture was warmed to rt, and stirred for 24 h; then H_2O (100 mL) was added to the stirred mixture. The CH_2Cl_2 phase was separated and dried ($MgSO_4$). Aromatic 2,3-diaminopyridine (1.7 mmol) was added to the CH_2Cl_2 phase. The mixture was stirred for 5 days at rt. The precipitate **8a** was collected and dissolved in EtOH (50 mL) and then refluxed for 3 hours. The precipitate **9a** was collected and crystallised from EtOH.

4-Benzoyl-1-phenyl-3-amino-*N*-(2-amino-3-pyridyl)pyrrolino-2,5-dione 8a. Light grey needles (210 mg, 32%), m.p. 197 °C. IR (ATR): 3328, 3297, 3242, 3157, 3082, 2952, 2853, 1773, 1721, 1645 cm^{-1}. ^{1}H NMR (300.13 MHz, DMSO-d_6): δ = 3.42 (br. s, 3H, HCl, H_2O), 5.75 (br. s, 2H, NH_2), 6.72 (dd, 1H, J = 7.8 Hz, J = 6.3 Hz, H-5-Py), 7.05 (dd, 1H, J = 7.8 Hz, J = 1.4 Hz, H-4-Py), 7.25–7.56 (m, 11H, H-Ar), 13.12 (br. s, 1H, NH). ^{13}C NMR (75.47 MHz, DMSO-d_6): δ = 97.98, 113.75, 119.93, 122.37, 126.97, 127.23, 128.49, 128.63, 129.98, 133.20, 133.58, 141.58, 144.77, 164.79, 170.35, 174.45, 187.09. MS-ESI: m/z 385. Anal. calcd for $C_{22}H_{16}N_4O_3$ + 0.05H_2O + 1.35HCl: C, 60.81; H, 4.05; N, 12.89%. Found: C, 60.80; H, 4.05; N, 12.93%.

3-Benzoyl-1-phenyl-1,4-dihydro-2*H*-pyrido[2,3-*b*]pyrrolo[3,2-*e*]-pyrazin-2-one 9a. Light orange needles (110 mg, 18%), m.p. 362 °C. IR (ATR): 3244, 3159, 3058, 2957, 1719, 1649, 1593 cm^{-1}. ^{1}H NMR (300.13 MHz, DMSO-d_6): δ = 7.42–7.59 (m, 11H, H-Ar), 7.87 (d, 2H, J = 6.9 Hz, H-2′,6′-benzoyl), 8.61 (dd, 1H, J = 6.58 Hz, J = 1.73 Hz, H-5), 8.63 (dd, 1H, J = 3.03 Hz, J = 1.73 Hz, H-7), 13.9 (br. s, 1H, NH). ^{13}C NMR (75.47 MHz, DMSO-d_6): δ = 94.77, 107.49, 122.66, 124.08, 127.46, 127.78, 128.86, 128.92, 131.75, 133.04, 138.84, 146.30, 147.31, 151.30, 165.94, 189.30. MS-ESI: m/z 367 (M^+ + 1). Anal. calcd for $C_{22}H_{14}N_4O_2$: C, 72.12; H, 3.85; N, 15.29%. Found: C, 71.60; H, 3.91; N, 15.07%.

Acknowledgements

We thank Grzegorz Trębacz for the quantum yield measurements and Anna Ostrowska for preparing Fig. 4–11. The research was carried out using the equipment purchased thanks to the financial support from the European Regional Development Fund in the framework of the Polish Innovation Economy Operational Program (contract no. POIG.02.01.00-12-023/08).

References

1 P. de Silva, H. Q. N. Gunaratne, Th. Gunnlaugsson, A. J. M. Huxley, C. P. McCoy, J. T. Rademacher and T. E. Rice, *Chem. Rev.*, 1997, **97**, 1515–1566.
2 J. F. Callan, A. P. de Silva and D. C. Magri, *Tetrahedron*, 2005, **61**, 8551–8588.
3 A. Loudet and K. Burgess, *Chem. Rev.*, 2007, **107**, 4891–4932.
4 E. M. Nolan and S. J. Lippard, *Chem. Rev.*, 2008, **108**, 3443–3480.
5 E. L. Que, D. W. Domaille and Ch. J. Chang, *Chem. Rev.*, 2008, **108**, 1517–1549.
6 C. Lodeiro, J. L. Capelo, J. C. Mejuto, E. Oliveira, H. M. Santos, B. Pedras and C. Nuñez, *Chem. Soc. Rev.*, 2010, **39**, 2948–2976.
7 G. Aragay, J. Pons and A. Merkoçi, *Chem. Rev.*, 2011, **111**, 3433–3458.
8 J. Wu, W. Liu, J. Ge, H. Zhang and P. Wang, *Chem. Soc. Rev.*, 2011, **40**, 3483–3495.
9 Y. Jeong and J. Yoon, *Inorg. Chim. Acta*, 2012, **381**, 2–14.
10 M. Dutta and D. Das, *TrAC, Trends Anal. Chem.*, 2012, **32**, 113–132.
11 M. Formica, V. Fusi, L. Giorgi and M. Micheloni, *Coord. Chem. Rev.*, 2012, **256**, 170–192.
12 S. C. L. Pinheiro, I. M. Raimundo Jr, M. C. Moreno-Bondi and G. Orellana, *Anal. Bioanal. Chem.*, 2010, **398**, 3127–3138.
13 M. C. Kimber, I. B. Mahadevan, S. F. Lincoln, A. D. Ward and E. R. T. Tiekink, *J. Org. Chem.*, 2000, **65**, 8204–8209.
14 V. V. S. Mummidivarapu, K. Tabbasum, J. P. Chinta and Ch. P. Rao, *Dalton Trans.*, 2012, **41**, 1671–1674.
15 Y. Zhang, X. Guo, W. Si, L. Jia and X. Qian, *Org. Lett.*, 2008, **10**, 473–476.
16 X. Zhou, B. Yu, Y. Guo, X. Tang, H. Zhag and W. Liu, *Inorg. Chem.*, 2010, **49**, 4002–4007.
17 H. Zhang, Q.-L. Wang and Y.-B. Jiang, *Tetrahedron Lett.*, 2007, **48**, 3959–3962.
18 J. Jiang, H. Jiang, X. Tang, L. Yang, W. Dou, W. Liu, R. Fang and W. Liu, *Dalton Trans.*, 2011, **40**, 6367–6370.
19 X. Zhou, Y. Lu, J.-F. Zhu, W.-H. Chan, A. W. M. Lee, P.-Sh. Chan, R. N. S. Wong and N. K. Mak, *Tetrahedron*, 2011, **67**, 3412–3419.
20 L. Xue, Ch. Liu and H. Jiang, *Org. Lett.*, 2009, **11**, 1655–1658.
21 T. Ghosh, B. G. Maiya and A. Samanta, *Dalton Trans.*, 2006, 795–801.
22 E. Korin, B. Cohen, Ch.-Ch. Zeng, Y.-Sh. Xu and J. Y. Becker, *Tetrahedron*, 2011, **67**, 6252–6258.
23 B. Wilson, L. Gude, M.-J. Fernández, A. Lorente and K. B. Grant, *Inorg. Chem.*, 2005, **44**, 6159–6173.
24 Y. Wang, X.-Y. Hu, L. Wang, Zh.-B. Shang, J.-B. Chao and W.-J. Jin, *Sens. Actuators, B*, 2011, **156**, 126–131.

Published on 11 October 2013. Downloaded by Laurentian University on 04/11/2013 00:26:56.

25 M. S. Park, K. M. K. Swamy, Y. J. Lee, H. N. Lee, Y. J. Jang, Y. H. Moon and J. Yoon, *Tetrahedron Lett.*, 2006, **47**, 8129–8132.
26 C. Bazzicalupi, A. Bencini, I. Matera, S. Puccioni and B. Valtancoli, *Inorg. Chim. Acta*, 2012, **381**, 162–169.
27 H. N. Lee, H. N. Kim, K. M. K. Swamy, M. S. Park, J. Kim, H. Lee, K.-H. Lee, S. Park and J. Yoon, *Tetrahedron Lett.*, 2008, **49**, 1261–1265.
28 M. Taki, Y. Watanabe and Y. Yamamoto, *Tetrahedron Lett.*, 2009, **50**, 1345–1347.
29 A. Rocha, M. M. B. Marques and C. Lodeiro, *Tetrahedron Lett.*, 2009, **50**, 4930–4933.
30 H.-H. Wu, Y.-L. Sun, Ch.-F. Wan, Sh.-T. Yang, Sh.-J. Chen, Ch.-H. Hu and A.-T. Wu, *Tetrahedron Lett.*, 2012, **53**, 1169–1172.
31 J. Zhang, H. Cui, M. Hojo, Sh. Shuang and Ch. Dong, *Bioorg. Med. Chem. Lett.*, 2012, **22**, 343–346.
32 P.-E. Danjou, J. Lyskawa, F. Delattre, M. Becuwe, P. Woisel, S. Ruellan, S. Fourmentin and F. Cazier-Dennin, *Sens. Actuators, B*, 2012, **171–172**, 1022–1028.
33 B. Wang and E. V. Anslyn, in *Chemosensors*, ed. D. Lee, A John Wiley & sons. Inc. Publication, Singapore, 2011, pp. 41–64.
34 M. S. Nasir, Ch. J. Fahrni, D. A. Suhy, K. J. Kolodsick, Ch. P. Singer and T. V. O'Halloran, *J. Biol. Inorg. Chem.*, 1999, 775–783.
35 K. Ostrowska, E. Piegza, M. Rąpała-Kozik and K. Stadnicka, *Eur. J. Org. Chem.*, 2012, 3636–3646.
36 K. Jamroży, K. Szymoniak and K. Ostrowska, *Heterocycles*, 2008, **75**, 2275–2282.
37 K. Ostrowska, K. Szymoniak, M. Szczurek, K. Jamroży and M. Rąpała-Kozik, *Tetrahedron*, 2011, **67**, 5219–5227.
38 R. Satapathy, Y.-H. Wu and H.-Ch. Lin, *Org. Lett.*, 2012, **14**, 2564–2567.
39 Q. Zhao, R.-F. Li, Sh.-K. Xing, X.-M. Liu, T.-L. Hu and X.-H. Bu, *Inorg. Chem.*, 2011, **50**, 10041–10046.
40 J. Du, J. Fan, X. Peng, H. Li and Sh. Sun, *Sens. Actuators, B*, 2010, **144**, 337–341.
41 Nonius, *COLLECT*, Nonius BV, Delft, The Netherlands, 1998.
42 Z. Otwinowski and W. Minor, in *Methods in Enzymology, Macromolecular Crystallography, Part A*, C. W. Carter, Jr and R. M. Sweet, ed., Academic Press, New York, 1997, vol. 276, pp. 307–326.
43 G. M. Sheldrick, A short history of SHELX, *Acta Crystallogr., Sect. A: Found. Crystallogr.*, 2008, **64**, 112–122.
44 Agilent, *CrysAlis PRO*, Agilent Technologies UK Ltd, Yarnton, England, 2011.
45 L. J. Farrugia, *J. Appl. Crystallogr.*, 1999, **32**, 837–838.
46 L. J. Farrugia, ORTEP-3 for Windows - a version of ORTEP-III with a Graphical User Interface (GUI), *J. Appl. Crystallogr.*, 1997, **30**, 565–568.
47 M. Nardelli, *J. Appl. Crystallogr.*, 1995, **28**, 659.
48 M. Nardelli, A. Musatti, P. Domiano and G. Andreetti, *Ric. Sci.*, 1965, **15**(II-A), 807.
49 G. A. Lawrance, *Introduction to Coordination Chemistry*, ed. A. John, Wiley & sons. Inc., Publication, 2010, pp. 127–131.
50 Ch.-Sh. Choi, K.-S. Jeon, W.-Ch. Jeong and K.-H. Lee, *Bull. Korean Chem. Soc.*, 2010, **31**, 1375–1376.
51 A. Demeter, T. Bérces, L. Biczók, V. Wintgens, P. Valat and J. Kossanyi, *J. Phys. Chem.*, 1996, **100**, 2001–2011.
52 P. Valat, V. Wintgens, J. Kossanyi, L. Biczok, A. Demeter and T. Berces, *J. Am. Chem. Soc.*, 1992, **114**, 946–953.
53 S. Periyaraja, A. B. Mandal and P. Shanmugam, *Org. Lett.*, 2011, **13**, 4980–4983.
54 Q.-Y. Cao, J. F. Zhang, W. X. Ren, K. Choi and J. S. Kim, *Tetrahedron Lett.*, 2011, **52**, 4464–4467.
55 D. Y. Han, J. M. Kim, J. Kim, H. S. Jung, Y. H. Lee, J. F. Zhang and J. S. Kim, *Tetrahedron Lett.*, 2010, **51**, 1947–1951.

 This journal is © The Royal Society of Chemistry and the Centre National de la Recherche Scientifique 2013